Geochemistry, Geophysics, Geosystems

RESEARCH ARTICLE
10.1029/2019GC008901

Key Points:

- Alaska convergent margin backstops are splay fault zones between the accreted prism and the continental margin framework
- These splay faults continue along the entire Alaska margin and occur at or near the updip end of the seismogenic zone
- The tsunami potential of backstop splay fault zones adds to considerations of tsunami hazards along the U.S. west coast

Supporting Information:

- Supporting Information S1

Correspondence to:
R. von Huene,
rhuene@mindspring.com

Citation:
von Huene, R., Miller, J. J., & Krabbenhoeft, A. (2021). The Alaska convergent margin backstop splay fault zone, a potential large tsunami generator between the frontal prism and continental framework. *Geochemistry, Geophysics, Geosystems*, *22*, e2019GC008901. https://doi.org/10.1029/2019GC008901

Received 14 JAN 2020
Accepted 27 AUG 2020

The Alaska Convergent Margin Backstop Splay Fault Zone, a Potential Large Tsunami Generator Between the Frontal Prism and Continental Framework

Roland von Huene[1], John J. Miller[2], and Anne Krabbenhoeft[3]

[1]U.S. Geological Survey, Emeritus, Moffett Field, CA, USA, [2]U.S. Geological Survey, Emeritus, Denver Federal Center, Denver, CO, USA, [3]GEOMAR Helmholtz Centre for Ocean Research, Kiel, Germany

Abstract The giant tsunami that swept the Pacific from Alaska to Antarctica in 1946 was generated along one of three Alaska Trench instrumentally recorded aftershock areas following great and giant earthquakes. Aftershock areas were investigated during the past decade with multibeam bathymetry, ocean bottom seismograph wide-angle seismic, reprocessed legacy, and new seismic reflection images. Summarized and updated here are previous papers and additional data. Tectonic structures collocated with aftershock area boundaries indicate possible lengths of rupture in future great earthquakes. NE aftershock area boundaries relate to subducted lower plate structures whereas the SW zone upper plate retains Beringian structural relicts. The lower to middle slope transition separating a stronger continental framework rock from a weaker accreted prism occurs along splay fault zones previously interpreted as backstops in seismic images. Damage zones along splay faults are generally 1-km-wide dipping typically 21°. Splays form slip paths from the plate interface to the seafloor much shorter than the 3–4° dipping plate interface beneath the frontal prism. Associated seafloor vent structures indicate overpressured fluids at depth. Splay fault dip and its rigid hanging wall impart greater seafloor uplift than the accreted prism per unit of slip making them effective tsunami generators. Backstop splay fault zones (BSFZs) run along the entire Alaska Trench. Beneath the frontal prism, active bend faults add rugosity to the plate interface and km high relief is commonly imaged in reprocessed legacy and new seismic data. The 1946 Unimak great (M8.6) earthquake epicenter is located near the BSFZ.

Plain Language Summary Along the Alaska Trench lower slope, a tectonic boundary termed a *backstop* was recognized in seismic reflection images ~40 years ago. Backstops are envisioned as mechanical boundaries along which weak sediment accreted against a buttress of stronger more rigid rock. Upper parts are seismically imaged but deeper parts are hidden by the overprint of multiple reflections and are not resolved convincingly in two-dimensional seismic reflection data. Legacy (1970–1990) seismic data were reprocessed with later more developed software and combined with high-resolution bathymetry. The combined data reveal that backstops are *splay fault zones*, similar to those off Nankai, Japan resolved in three-dimensional data. Models indicate that splay faults may generate giant tsunamis like the 1946 Pacific-wide tsunami that traveled from Alaska to Antarctica. The diversion of earthquake slipup splay faults could be helped locally by a rough interface separating oceanic from continental plates. Beneath the accreted prism, plate interface roughness was resolved with modern software. Splay faults run along the entire Alaskan margin and add a feature to consideration of trans-oceanic tsunamis reaching American west coasts and Hawaii.

1. Introduction

The converging Alaska margin extends from the Kenai Peninsula and Middleton Island to the western end of the Alaskan Peninsula at Unimak Island (Figure 1) where it transitions to the Aleutian Arc. Instrumental seismology recorded two great (M8–M9) and one giant (≥M9) earthquake along the Alaska margin. Main shocks were followed by aftershocks over areas thought to indicate the extent of rupture and segmentation of seismicity (e.g., Ruppert et al., 2007; Sykes, 1971). However, knowledge of tectonic barriers to earthquake rupture at segment boundaries was imprecise. Furthermore, only one M8 or M9 earthquake in the seismic cycle has been instrumentally recorded in each segment.

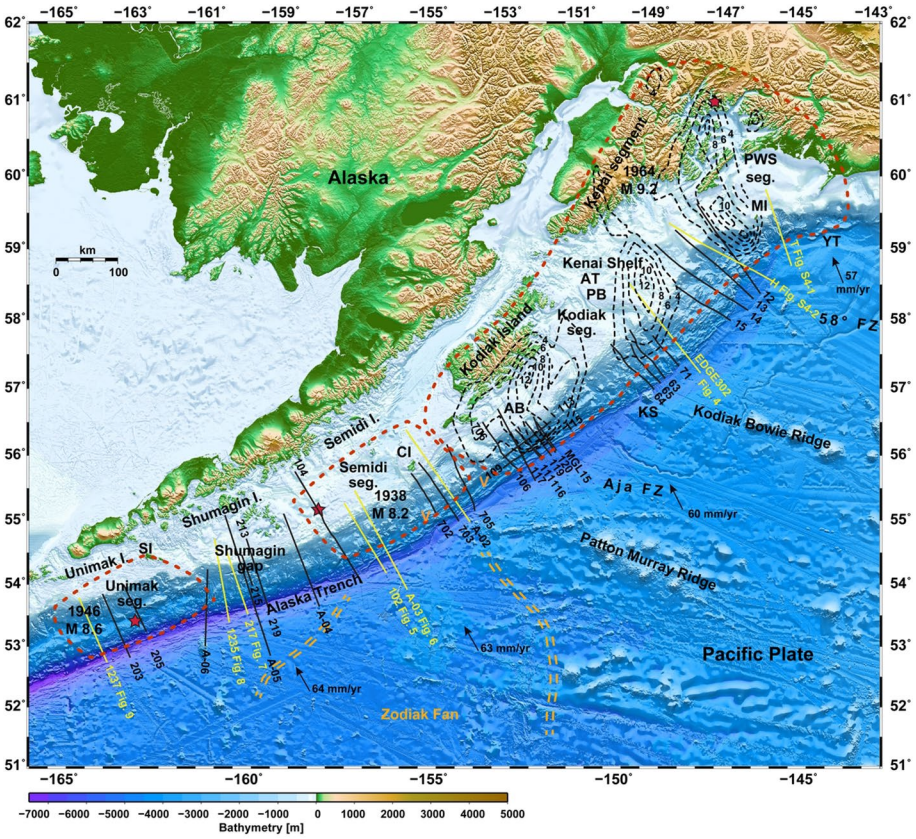

Figure 1. Earthquake rupture areas (enclosed with red dashed lines) indicated by aftershock distribution after ≥M8 earthquakes. Seismic transects are shown with lines and numbers (A- = ALEUT project, 1235 & 1237 = RV Ewing, MGL = RV Langseth, H & T = Hinchinbrook and Tact transects. Other lines are from S. P. Lee. Red stars = ≥M8 earthquakes epicenters (earthquake.usgs.gov/earthquakes/): 1964 earthquake slip contours (Ichinose et al., 2007) with dashed lines at 2-m contour intervals. PWS, Prince William Sound; YT, Yakutat terrane under a sediment cover; MI, Middleton Island; AT, Amatuli Trough; KS, Kodiak Seamount; PB, Portlock Bank; AB, Albatross Bank; CI, Chirikof Island; SI, Sanak Island; orange "v" indicates locations of vent in Figure 11, orange dashed double lines = Zodiak fan, bathymetry is from the GEBCO 2019 grid.

Each great and giant earthquake generated a trans-oceanic tsunami. Explanations of the tsunamigenic mechanisms were largely hypothetical because the margin's tectonic structure was only beginning to be explored geophysically in the 1970s (e.g., Bruns et al., 1987, von Huene et al., 1987). Surveys in the 1990s added patches of multibeam bathymetry and two wide-angle seismic transects. Follow-on publications since 2011 contain bathymetric compilations integrated with reprocessed legacy seismic images, wide-angle seismic tomography, and improved acquisition with RV Langseth (Figures 1 and 2). These form a new data set for investigation of upper and lower plate structure along the Alaska margin. Also available are publications of regional GLORIA backscatter images, vertical gravity gradients, residual gravity, and compilations of seismicity, all of which expand available data.

This contribution addresses questions of whether aftershock area boundaries correspond to large tectonic features and the difference in tectonic structure from subducted relief within each segment's borders. It is an updated summary of investigations during the past decade with emphasis on a splay fault relevant to tsunami hazard assessments (Bécel et al., 2017; Kirby et al., 2013; Krabbenhoeft et al., 2021; Li et al., 2015; Ryan et al., 2013; von Huene et al., 2012, 2015, 2016, 2019). We begin with historic development of convergent margin concepts applied in Alaska margin investigations, then show features that single out the splay fault zone from imbricate thrusts at the Nankai margin. We define earthquake aftershock segment boundaries that divide Alaska margin geology in each segment and identify Nankai-type splay faults. Large fluid vent structures associated with splay faults are shown, and the growth of lower plate relief in the subduction

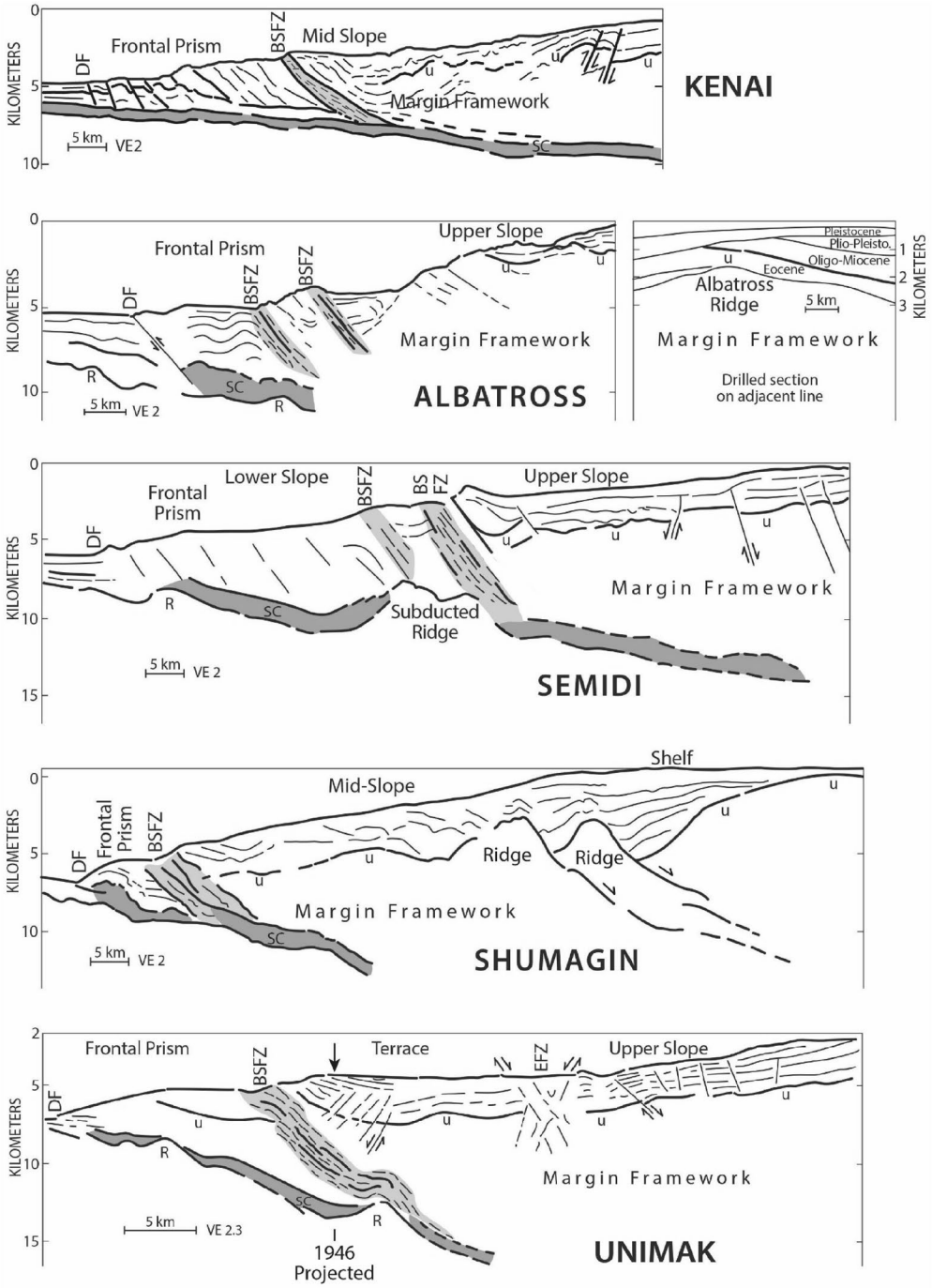

Figure 2. Line drawings of composite tectonic features in seismic images of previous papers. Unconformity age at the shelf edge is constrained with drill samples from Albatross ridge (Turner et al, 1987, p. 341; Winston, 1983) and on shore. Kenai sketch is from EDGE (von Huene et al., 1998). ALBATROSS images lack a semi-coherent Oligo-Miocene unconformity reflection (Krabbenhoeft et al., 2021). In the SEMIDI section, a large subducted ridge is sketched after line 03 (von Huene et al., 2015). The SHUMAGIN image contains a buried extensional structure similar to the exposed Unimak ridge in the Unimak segment (Bécel et al., 2017; von Huene et al., 2019). The UNIMAK section is after Ewing line 1237, (von Huene et al., 2016). The Aleutian mid-slope terrace begins here. R = subducting relief; BSFZ = backstop splay fault zone; U = Oligo-Miocene unconformity; DF, deformation front; EFZ , extensional fault zone; SC, subduction channel and the star marks the projected position of the 1946 M8.6 Unimak earthquake epicenter.

zone is discussed. Some interpretations in our previous papers are updated. A principal objective is to advance understanding of tsunami hazards and mechanisms.

1.1. A History of Investigations

Since the 1964 giant Alaska earthquake, a conceptual framework of Alaskan margin tectonics evolved as data acquisition increased. Seismic reflection images of the 1970s and 1980s resolved mostly shallow structure of the frontal prism and strata of the slope sediment cover. Few coherent reflectors beneath the mid-slope sediment cover were apparent. An explanation was that accreted sediment became a melange deformed beyond seismic reflection system resolution. Accreted trench sediment from trench to shelf was inferred from a constant accretionary conceptual model (e.g., Seely & Dickinson, 1977). A confidential industry seismic image located somewhere off the northern Kodiak group of islands showed seafloor ridges interpreted as thrust faults across the middle slope (Seely, 1977). However, research community surveys failed to find ridges landward of the accreted prism. Imaging showed only small segments of coherent shallow dipping reflections beneath the middle and upper slope sediment cover and explanations of structure were hypothetical. Within 20 km of the shelf edge are insular outcrops of an exhumed Mesozoic (?) metamorphic complex that forms the margin rock framework (Moore, 1972; Moore et.al., 1983). The relation of metamorphic complex and accreted prism was absent from geophysical data between the shelf edge and the prism.

A similar absence occurred across the Barbados volcanic island arc where geology is simpler. Accreted prisms must back against arc rock somewhere beneath the slope. Arcs were visualized as strong buttresses against which trench sediment accreted. Backstop was a term for this conceptual boundary (e.g., Byrne et al., 1988). Across the SW Alaska margin, an unclearly imaged buttress interface with the prism was an explanation for seismically imaged structure and an acoustic basement rock buttress rather than volcanic arc rock (e.g., Bruns et al., 1987; Figure 13). The upper and middle slope high-velocity acoustic basement that unconformably underlies the slope sediment cover could be older framework rock as found beneath the shelf. This was allowable since industry drill hole sampling near the shelf edge off Kodiak Island bottomed in Eocene sedimentary rock overlain unconformably by middle Miocene sediment (Turner et al., 1987). Samples yielded fossils indicating mid to shallow water Eocene deposition, consistent with erosion of the unconformity. The Eocene to Miocene unconformity continues over the shelf edge and across part of the slope in an industry seismic image (Winston, 1983). This regional unconformity continues down the slope and breaks up adjacent to the backstop in a deformed zone of poorly coherent steeply dipping reflections (Bruns et al., 1987). The middle to lower slope deformed zone was interpreted as part of the backstop at the seaward end of margin framework rock forming a buttress against which the prism accreted.

Alaskan backstops are transitions between the middle slope acoustic reflection patterns and imbricate frontal prism structure. Single strong backstop reflections were depicted by a line in conceptual diagrams but they were rare. As multibeam bathymetry was acquired, backstop structures in the series of Alaskan seismic images (Figure 1) were linked with detailed backstop seafloor morphology. In the transition zone, the seafloor steepens and displays local fresh fault scarps. In multibeam acquired morphology, backstop scarps differ from the multibeam ridges of frontal prism (cf. Krabbenhoeft et al., 2021). Transitions commonly separate a more rigid appearing margin framework morphology from accreted prism ridges (e.g., von Huene et al., 2012). Frontal prisms are narrower than commonly envisioned and form the first 15–30 km of the margin. In well-constrained two-dimensional (2D) mass balance calculations, the accreted prism volume equals that delivered by plate convergence during roughly 1–3 Myr (e.g., von Huene et al., 1998). The frontal prism is probably shaped mostly by Quaternary tectonism, yet at the shelf edge, a much older Eocene sediment unconformably overlies Mesozoic metamorphic rock (Moore et.al., 1983). This large gap in ages was poorly understood. The conceptual framework applied in this paper has evolved with progressively improved seismic resolution from the constantly accreting prism concept (e.g., Seely & Dickinson, 1977) to trench sediment accreting against a basement buttress (e.g., Clift & Vannucchi, 2004) to a backstop transition zone. The current step in this progression comes with applying the understanding from the three-dimensional (3D) seismic images across the Nankai margin that show with convincing resolution the structure of a splay fault zone (G. F. Moore et al. 2007). We posit that Nankai-type splay fault zones are found

along the entire Alaska margin despite lack of a 3D seismic transect. Alaska seismic images resolve many features common to the Nankai-type structure (Figure 2). A motivation in this investigation is the splay fault's potential to generate tsunamis more efficiently than generation involving only frontal prisms (Lotto et al., 2019; Wendt et al., 2009).

The Nankai type-example is a ~5-km-wide thrust fault zone about half of which has incoherent diffuse reflectivity (G. F. Moore et al., 2007, seismic images). It cuts across imbricate fault slices of the accreted prism that forms the splay fault footwall. The hanging wall is formed by the middle prism. The hanging wall basement is topped by a transgressive angular unconformity upon which a 1.0 to 1.5-km-thick, finely bedded, flat lying Kumano Basin sediment sequence rests. Basin strata are essentially undeformed and at site C0002, are 2.1 ± 0.4 Myr old. A lack of deformation in sediment strata indicates hanging wall uplifted as a semi-rigid slab during Quaternary splay fault slip. The splay fault forms seafloor scarps locally up to 1-km high with a morphology as recent as that of the frontal prism faulting along the deformation front. The splay fault damage zone cuts off the decollement as well as reflections in the hanging wall. At the plate interface, a ~2-km-wide fault damage zone merges with the subducting sediment layer and becomes part of the layer on ocean basement. Rigid hanging wall basement forms a backstop against which prism sediment accreted (e.g., G. F. Moore et al., 2007].

The Nankai splay fault zone was highlighted with the term “splay” rather than out of sequence fault (G. F. Moore et al., 2007). Thrust faults have been termed splay faults in shelf areas far from active accreted prisms separated across backstops as at the Nankai type-locality. For clarity, we apply the term “backstop splay fault zone” (BSFZ) to show the similarity with the Nankai-type example of splay faulting (G. F. Moore et al., 2007).

Prior to the Nankai 3D transect, splay faults were commonly considered imbricate thrust units of accreted prisms. Resolved from structural relations at Nankai is that the splay fault zone consists of fault damaged rock whereas accreted prisms are fault bounded trench and slope sediment units. To see that difference in seismic displays requires high resolution imaging such as that afforded by 3D data. Features that point to a Nankai-type structure are a lower to middle slope steepened seafloor slope transition, and when active, scarps where the fault zone emerges at the seafloor. The fault zone is commonly wider than the 1-km-thick trench sediment turbidites detached in imbricate fault bend folds of the prism. The splay fault zone commonly truncates foot wall and hanging wall strata on either side. Locally, upslope seismic patterns differ from those of the downslope prism pattern. Where plate interface primary reflectivity is not masked by the seafloor multiple, the critical juncture showing splay fault zone continuity with the plate interface sediment layer is resolved. Mid-slope terraces behind a ridge commonly pinpoint seafloor emergence of the splay fault (cf. G. F. Moore et al., 2007). Not all of these defining features are consistently imaged along the Alaska convergent margin perhaps because of structural differences and a structural continuity along strike.

2. Geologic Structure Along Borders of >M8 Earthquake Aftershock Areas.

Aftershock distribution following three great earthquake ruptures was recorded instrumentally along the Alaska convergent margin (Sykes et al., 1980). From NE to SW they are the Kodiak, Semidi, and Unimak aftershock areas (Figure 1). We divide the Kodiak area into a Kenai and Albatross sector. The Shumagin Islands area, without a great earthquake (≥M8) is bounded by distal aftershocks of the adjacent Semidi and Unimak areas (Figure 1). Geophysical data indicates structure transverse across the margin in the aftershock boundary zones of each area (Krabbenhoeft et al., 2021; Miller et al., 2014; von Huene et al., 2012–2019).

The lower plate modifies a basic Alaska margin structure by subduction of three prominent morphological features: the Kodiak-Bowie, and the Patton-Murray seamount chains (Figure 1) and the subducted Yakutat terrane (Figures 1 and S4). These features enter the subduction zone along a NE trajectory because of the plate convergence vector's 60° angle with the trend of ridges and fracture zones. That causes a NW entry area migration along the Semidi and Kodiak segments (Stock & Molnar, 1988) (Figure 1). Subducting relief leaves various erosional features that were resolved once multibeam bathymetry was acquired. Locally, accreted prisms and backstops of the Alaskan margin are severely disrupted but a stronger and thicker margin framework is less impacted as shown by greater resistance to erosion than the frontal prism in multibeam bathymetry.

The Shumagin Gap and Unimak earthquake segments were affected by another event that left diagonal trending structure across the upper plate paralleling the Beringian continental slope. It was probably inherited after Eocene capture of the Bering subduction zone and construction of the Aleutian Arc (e.g., J. C. Moore, 1972; Scholl, 2007).

2.1. The Kenai – Yakutat Terrane Boundary

At its NE end, the Alaska convergent margin begins at the trailing flank of the Yakutat terrane (Figure 1) (e.g., Bruns, 1983; Fruehn et al., 1999) (supporting information S4). East of the trench axis, the terrane's unsubducted trailing flank forms the central Gulf of Alaska margin (Figure 3). At the Alaska Trench it subducts beneath the Kenai shelf. Even at 12–18 km depth (Brocher et al., 1994), the subducted trailing flank EW trend is paralleled by two EW trending morphological features, Portlock Bank and Amatuli Trough, (Figures 1 and 3) (GEBCO 2019 grid). The Yakutat's EW trending slope magnetic anomaly continues west of Middleton Island beneath the Kenai shelf (Figure 3). The overlying Kenai sediment section collapses behind the subducted Yakutat trailing flank. This oversteepened slope first experiences gravity failure followed by compressional folding from plate convergence (Figure 3 and Figure S4-1). Seafloor expression of the slope anomaly also continues across the shelf to the Kenai Peninsula as an EW trending shallow lineament (Figure 3) (Zimmermann & Prescott, 2015). A separation of the 1964 aftershocks into a Prince William and a Kodiak segment occurs across these features. The tectonic elements of this juncture are shown in the reprocessed TACT and Hinchinbrook seismic images (supporting information S4). These features indicate tectonic structure at the NE end of the Alaska convergent margin corresponding with the boundary between two 1964 earthquake rupture areas (Ichinose et al., 2007). The BSFZ at this juncture is shown in the TACT line (Figure S4-1) where debris from slope failure is thrust against the continental framework to form a small frontal prism. Farther SW, the Hinchinbrook line shows a frontal prism and the collapsed margin framework rock thrust faulted by contractile deformation after removal of the Yakutat terrane (see supporting information S4).

2.2. Kodiak – Semidi Boundary

Aftershock areas of the 1938 M8.2 Semidi and 1964 M9.2 Kodiak earthquakes meet in a deformed area of the upper plate above past and currently subducting complex lower plate relief (Krabbenhoeft et al., 2021;

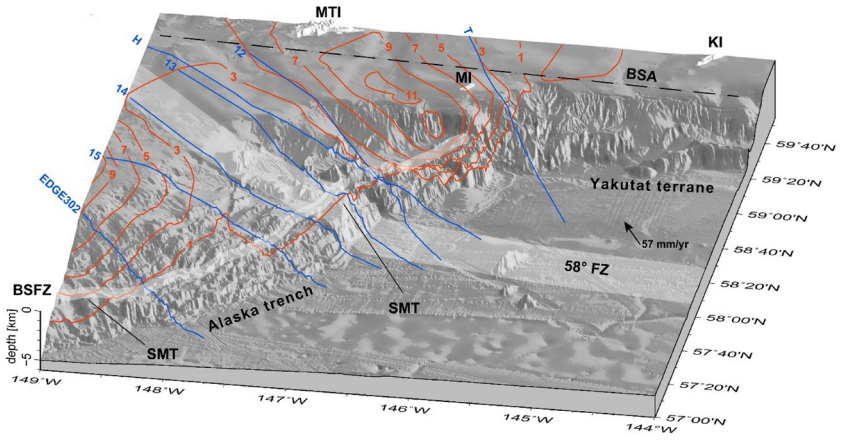

Figure 3. Perspective view of the Kenai sector created from multibeam bathymetric surveys incorporated into a GEBCO compilation (GEBCO 2019 grid). Multibeam data resolve the contrasting morphologies of the accretionary Kodiak margin (left) and the Yakutat terrane trailing flank marked by slide scars and an eroding slope (right). The light-colored corridor represents an approximated path of the buried and subducted 58° fracture zone. Red 2 m. Slip contours of the M9.2, 1964 Alaska earthquake are from Ichinose et al, (2007). BSFZ corridor, the surface trace of the Backstop Splay Fault zone; SMT, subducted seamount; BSA, Bathymetric trace above the buried Slope Anomaly magnetic body; MI, Middleton Island; MTI, Montague Island; KI, Kayak Island; H & T, Hinchinbrook and Tact seismic transects, other lines are from S.P. Lee cruises.

von Huene et al., 2012). Here multiple lower plate features subduct including Patton-Murray ridge and Aja fracture zone (Figure 1). They project to intersect the subducted Kula-Pacific ridge beneath the margin middle slope. The subducted apex of Zodiak fan is probably at a pass through these features for 10 Myr, and would be the fan head sediment entry point. We infer this from projection of several sediment channels that fed lobes of the fan (Stevenson & Embley, 1987). In the upper plate, embayments and transverse furrows across the middle slope parallel the plate convergence vector like those left by currently subducting seamounts (Krabbenhoeft et al., 2021). The complex lower plate relief and upper plate tectonic disruption are likely candidates for a barrier area that arrested slip propagation along the plate interface. Aftershocks ≥M5 were concentrated NE of this area during the 1964 post seismic period and heightened seismic activity continues (Krabbenhoeft et al., 2018, Figure 9) (http://www.aeic.alaska.edu/html_docs/db2catalog.html).

2.3. Semidi – Shumagin Boundary

At the SW limit of the 1938 M8.2 aftershocks, the Semidi and Shumagin segment's morphologies are interrupted by a broad morphological transition and a 20° change in regional trend (Figure 1). The subsurface structure here is undocumented. A 90-km-long NE trending transverse canyon in the boundary area (Figure 1) appears tectonically controlled by upper plate structure. Within the transition, GLORIA images display rough seafloor patches (U.S. Geological Survey Open-File Report 2010–1332). Seaward of the trench axis the seafloor is devoid of relief that would cause a rugose plate interface. Bend fault escarpments adjacent to the deformation front are only revealed in high resolution multibeam bathymetry and GLORIA images (Shillington et al., 2015).

2.4. Unimak-Shumagin Boundary

The Unimak M8.6 1946 earthquake aftershocks end at the diagonal trending Sanak Island structural zone (Lopez & Okal, 2006). The Sanak subseafloor structures resolved geophysically extend across the shelf and down the upper slope (Bruns et al., 1987; von Huene et al., 2018). Included in this structural zone is the ~40-km-wide Sanak Islands platform adjacent to the 170-km long and up to 7-km deep Sanak Basin. The diagonal Sanak morphological trend continues beyond the shelf edge to the middle slope indicating a continuation of margin framework basement toward the frontal prism (GEBCO 2019 grid). Its trend appears in the residual gravity map of Bassett and Watts (2015) where it can be traced across the Alaska Peninsula into the Bering Sea. This major structure is considered a vestige of the Paleogene Alaska–Bering margin juncture because of its Bering margin rather than Alaska Trench orientation (Bruns et al., 1987; J. C. Moore, 1972; Scholl, 2007).

At Unimak Pass, there are few geophysical data to indicate a boundary geology that could arrest great earthquake seismic slip. An embayment into the upper slope but not in the frontal prism suggests possible tectonic disruption by subducting relief predating the accreted prism. Absence of robust transverse morphology suggests a weak boundary to earthquake rupture arrest.

In summary, borders of great and giant earthquakes aftershock area are collocated with upper plate zones of tectonism and locally, lower plate relief. In the upper plate they are deformed transverse rather than trench parallel structural zones (cf. Bruns et al., 1987; Fisher & Holmes, 1980) except for two boundaries without sufficient geophysical information to image tectonic structure.

3. BSFZ Images Across Aftershock Areas

The three instrumentally recorded earthquake aftershock areas generated transoceanic tsunamis. The Unimak Segment is legendary for the 1946 earthquake that generated the largest Alaskan/Aleutian tsunami ever recorded (Fryer & Tryon, 2005; Okal et al., 2002). The 1938 Semidi segment earthquake was not highly tsunamigenic because its hypocenter was deep and distant from the margin front. The 1964 giant Alaska earthquake's Kodiak segment had two asperities (Figure 1) with shallow slip large enough to generate the tsunamis that damaged the Vancouver and U.S. west coasts. The southwest Kodiak asperity slip propagated

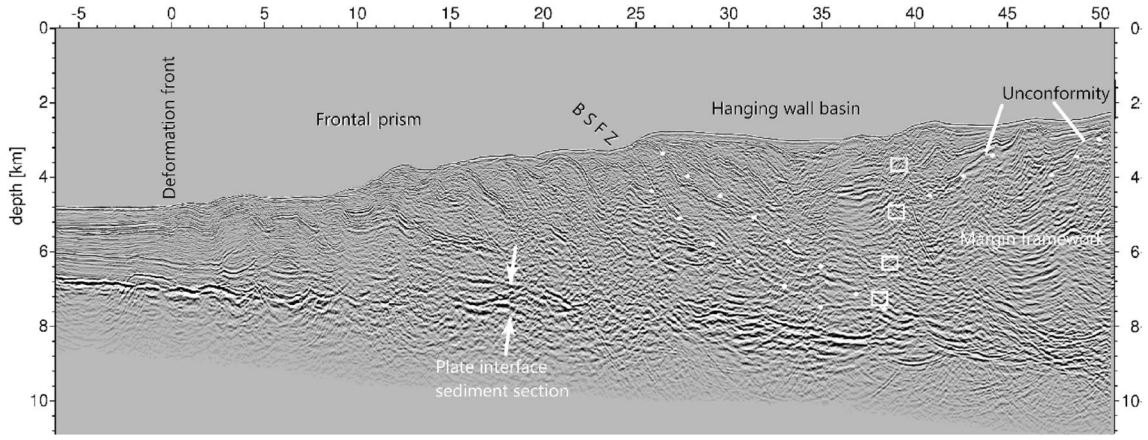

Figure 4. Prestack depth migrated image of the EDGE line in the Kenai sector. Landward verging structure in the frontal prism contrasts with the margin framework seaward vergence. Truncation of the unconformity and margin framework reflection approximate the margin's face after removal of a former frontal prism during subduction of the Yakutat terrane. White dots are along the BSFZ and boxes approximate the eroded face (after von Huene et al., 1998) (enlargement displays structure more clearly).

to the trench axis (Krabbenhoeft et al., 2021). Along the Semidi segment, the giant 1788 tsunami predating instrumental seismology is known from an anecdotal account and is supported by studies of sedimentary sequences on Kodiak and Chirikof Islands (Briggs et al., 2014, Nelson et al., 2015; Shennan, 2014). We summarize recent publications and reinterpret some points in accord with current information.

3.1. Kodiak Segment

In the Kodiak segment, aftershocks of the 1964 giant earthquake extended from Middleton Island to the southern limits of the Kodiak group of Islands. Kodiak Seamount in the trench axis begins a zone of disrupted bathymetry crossing the slope above the subducting Kodiak Bowie Ridge (Figure 1) (Krabbenhoeft et al., 2021; Figure S1). Although aligned bathymetric features across the middle shelf in the vertical gravity gradient are vague, the Kodiak Bowie Ridge trend projects into a southern 1964 earthquake asperity at the insular coast (Ichinose et al., 2007). The Kodiak Bowie trend separates a NE Kenai sector from a SW Albatross sector (Figure 1). Each sector includes an asperity of the 1964 earthquake and slip is calculated with a model that includes seismicity, tsunami, and geodetic observations (Ichinose et al., 2007, areas M2 and M3).

The 1964 Kenai asperity, north of Kodiak Seamount, coincides with magnetic anomalies marking the EW trending 58° fracture zone (Flueh & von Huene, 1994; Schwab et al., 1980]. The fracture zone anomalies extend ~140 km across the ocean basin and subduct at a 60-km-wide embayment into the lower slope (Figure 3, Figure S4–3). On the shelf, the fracture zone trend is continued by Amatuli Trough and Portlock Bank (Zimmermann & Prescott, 2015). Slip contours of the 1964 Kenai asperity across the shelf propagate down the continental slope to the BSFZ and stop before entering the trench axis (Figure 1) (Ichinose et al., 2007).

The EDGE line seismic image was developed from data acquired with a commercial vessel (Moore et al., 1991) and was prestack depth migrated and balanced (von Huene et al., 1998) (Figure 4). A backstop at the landward termination of the accreted prism was interpreted from dipping reflections of a 2 to 4-km-wide fault zone that truncates strata on either side. Its dynamic significance as a tsunami generating feature was not recognized at the time. Wide angle data (Ye et al., 1997) show an increased horizontal V_p gradient below 2-km depth across the BSFZ. Five seismic images northeast of the EDGE line and multibeam bathymetry indicate a backstop extending to the northeastern Kenai segment boundary (Figure 3) (Fruehn et al., 1999). In the EDGE image, the shelf sediment section on an Eocene to Miocene unconformity was followed ~25 km down the continental slope before deformation interrupted continuity and prevented correlations across faults (Figures 2–4). Beneath the sediment cover, margin framework rock is inferred. The

trench axis sediment adjacent to this segment is 2-km thick, and the lower ~1-km thick subducted sediment covers basement relief commonly 0.5-km high.

The Kenai sector's slope landward of the BSFZ contains ridges and valleys oriented parallel to the margin (Figure 3) proposed to have formed in the wake of the subducting Yakutat terrane (Fruehn et al., 1999). Mass wasting material in the wake is inferred to become imbricated into ridges orthogonal to the convergence vector (see supplemental section S4). A BSFZ morphology extends along the whole sector (Figure 3, Figure S4-3). It is clearly imaged in three lines and allowable in five other seismic images (Fruehn et al, 1999; von Huene et al., 1998]. As the Yakutat terrane trailing flank migrated past the deformation front, the frontal prism rebuilt. Southwest of the ridge and valley morphology, the area appears little affected by Yakutat terrane subduction. Here the BSFZ is associated with a low ridge about 25–30 km landward of the trench axis.

In the Albatross sector, structure appears unaffected by subduction of the Yakutat terrane. The 1964 earthquake's Albatross asperity rupture began near the Kodiak shore on a projection of the subducted Kodiak-Bowie Ridge (Figure 1). Slip contours extend south across the shelf subparallel to the convergence vector ending at the trench axis. Near the trench, a 14 m peak slip contour falls on the BSFZ indicating probable activation during generation of the 1964 tsunami (Krabbenhoeft et al., 2021).

In the Albatross sector, a slip maximum is collocated with concentrated aftershocks ≥M5 and heightened seismic activity continues. A grid of normal incident seismic images supported by wide-angle data provides quasi 2.5 D coverage. Beneath the trench floor, ~3-km-thick sediment subducts and beneath the accreted prism it modulates oceanic crust roughness which smooths the overlying plate interface (Krabbenhoeft et al., 2021). The BSFZ ridge separates steeper middle and upper slopes from shallower dipping lower slopes of the frontal prism. These two contrasting seafloor morphologies; a shallow dipping lower slope with trench-parallel ridges and a steeper rough middle and upper slope with more competent rock and a higher seismic velocity are characteristic of the Alaska margin.

3.2. Semidi Segment

Unique to the Semidi segment is a 160-km long, 5-km wide embayment eroded into the frontal prism between lines 703 & 102 (Figures 1 and 5). The long and little modified extensive embayment indicates erosion by a long margin parallel seafloor ridge (von Huene et al., 2015). Subduction of the inferred Kula Pacific ridge and currently the Patton-Murray ridge removed a frontal prism and has left truncated strata near the trench axis. Paralleling the embayment up slope is a 1-km-high mid-slope ridge where the BSFZ emerges. The Patton-Murray ridge presently subducts along the northeast end of the embayment and its trend di-

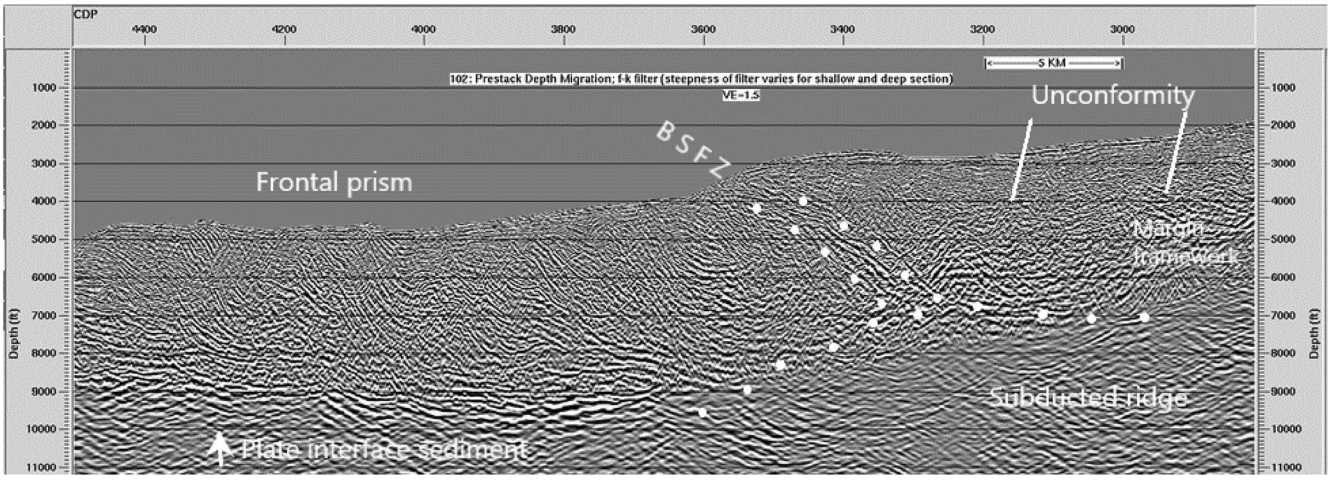

Figure 5. Legacy line L-8-81-WG 102 prestack depth migrated. The BSFZ bends over a subducted ridge approximated with white dots. BSFZ seafloor escarpment is 1+ km high.

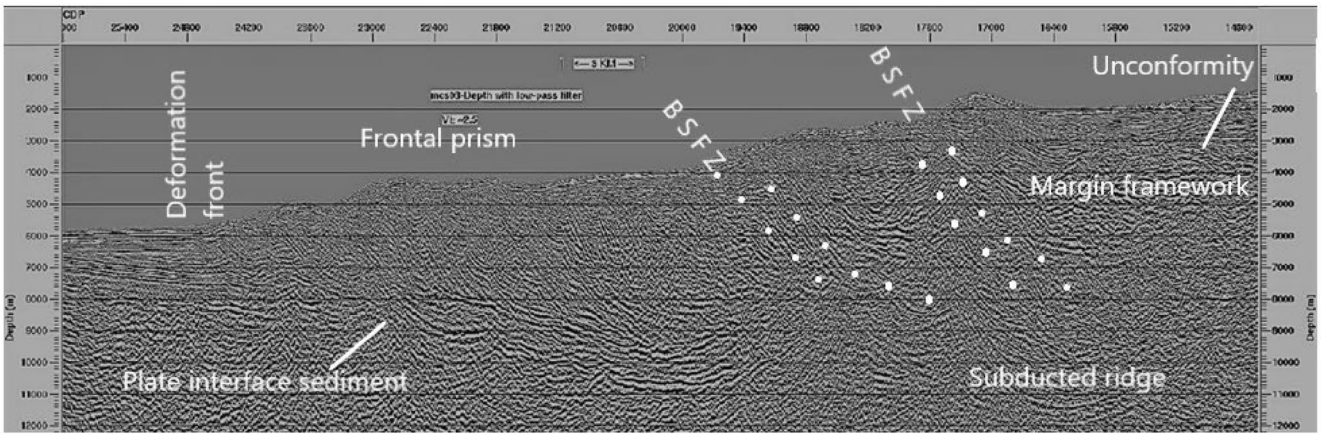

Figure 6. ALEUT 03. A morphologically rough subducted ridge is interpreted from: 1) disjointed and scattered reflections below the deep end of the BSFZ strata, 2) reflections end and plate interface strata are upturned beneath the seaward BSFZ below which reflectivity scatters (cdp 20,000), and 3) short reflections indicating a rough surface along the periphery of the obscured ridge reflectivity. The multiple cuts the right corner of this illustration. Enlargement improves clarity of structural detail.

verges from the subducted trench-parallel ridge. Plate reconstruction indicates that the Patton-Murray ridge and Aja fracture zone have migrated northeastward along the Semidi margin during the past ~1.5 Ma (von Huene et al., 2015, their Figure 6).

The Semidi BSFZ ridge is 4 to 5-km wide and 140-km long, broken at ~20 km intervals by oblique lineaments. It is little modified by erosion except for one or two deep structurally controlled canyons and small rills. The underlying subducted basement ridge associated with the BSFZ could be up to ~3-km high in the ALEUT 03 seismic image (Figures 5 and 6). The image of this deeply buried ridge is diffuse, and its presence is derived from the surrounding strata that bend over it. At the BSFZ area, line ALEUT 03 crosses a meandering seafloor channel whose morphology probably scattered seismic signals diminishing strong reflections from the deep lower plate ridge known from legacy data (von Huene et al., 2015). This can help explain the lack of a clear image in ALEUT 03 (Figure 6). In addition, the en' echelon BSFZ ridges add to geophysical image complexity. Free-air gravity anomalies (Bassett & Watts, 2015) are consistent with a subducted ridge. The basement foundation of this seafloor ridge is most likely the subducted Kula-Pacific Ridge (Stevenson & Embley, 1987).

3.3. Shumagin Gap Segment

The Shumagin gap is bounded by aftershock area borders of adjacent segments. It extends from Sanak Island northeastward to a short distance beyond the Shumagin group of islands, an area approximately the same size as adjacent great earthquake ruptures. Its potential to rupture in a great earthquake and generate a large tsunami, has been argued since attention was drawn to it by Sykes [1971]. Modeling indicates it might be capable of a great earthquake (Zheng et al., 1996), but Witter et al., (2014) found evidence that the Shumagin gap has been an area of persistent creep for at least 3,400 years. Geodetic observations show a lack of strain in the SW consistent with a creeping dynamic (Fournier & Freymueller, 2007). Its continental slope protrudes seaward of adjacent segments but its frontal prism is narrower than average widths on adjacent segments. Embayments into the deformation front from subducting relief are absent, consistent with the adjacent smooth seafloor; however, seismic data image subducted relief (Figures 7 and 8). This segment's morphology changes from a rugged SW half to a smoother NE half. Seismological data are also divided into two parts with different plate configurations (Hudnut & Taber, 1987). Multibeam bathymetry (Lewis et al., 1988) and GLORIA, display a continuous BSFZ. An uncommon buried extensional fault zone beneath the upper slope (Figure 2) adds to the unusual nature of the segment (Bécel et al., 2017). Down slope canyons and intervening morphological lobes of the upper and middle slope end abruptly along the

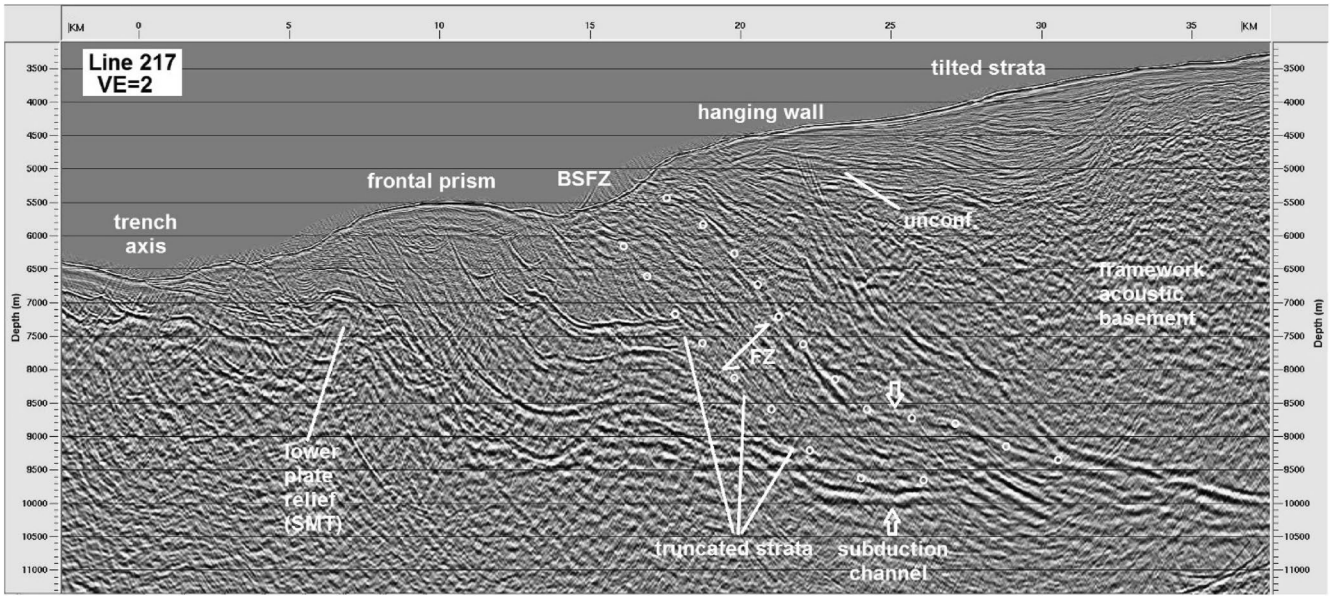

Figure 7. Legacy line 217 with a backstop splay fault zone (BSFZ) marked by truncated strata on either side. The fault damage zone continues into the subducting lower plate sediment layer. Unconformity in the hanging wall continues to the shelf edge.

BSFZ ridge indicating recent uplift. This segment's enigmatic dynamic indicators are also apparent in seismic and bathymetric observations with improved resolution.

Legacy seismic images across the Shumagin segment show a juncture of the BSFZ with the plate interface (Figure 7). The 5 km rather than 7 to 9-km depth of the juncture eliminates interference from the seafloor multiple, and perhaps structure is largely 2D which optimizes 2D imaging of structure.

Beneath the frontal prism the plate interface has 1-km-high relief. In seismic images the incoming ocean seafloor is relatively smooth but beneath the frontal prism abundant relief is imaged. Down dip of the BSFZ, the short well imaged plate interface strata are smooth. The splay truncates strata of the frontal prism along the footwall and where well defined, the damage zone is ~1.5-km thick. Plate interface dip = 10° + 2° and the splay dips 39° both of which are exceptionally steep.

3.4. Unimak Segment

The 1946 Unimak earthquake showed that giant Pacific-wide tsunamis can be generated along Alaska convergent margins, but the mechanics were not addressed with data for many years. Tsunami generation was first explained with simplified conceptual models (Okal & Hebert, 2007). Seismic transects of the 1980s, and multibeam bathymetry of the 1990s were acquired incrementally, earthquake seismology became more understandable, and more realistic tsunami generation scenarios were posited (cf. Bruns et al., 1987; Fryer & Tryon, 2005; Holbrook et al., 1999; Rathburn et al., 2009). Fryer and Tryon (2005) speculated that an unresolved splay fault might occur in the Unimak frontal prism. A BSFZ was later discovered (von Huene et al., 2016). The 1946 tsunami epicenter is on or near this BSFZ.

The 1946 Unimak earthquake produced both a near-field and far-field tsunami. The near-field tsunami's 42-m-high runup destroyed the Scotch Cap lighthouse. It was characteristic of a landslide source, possibly from a detached landslide block, but the detachment is not dated (von Huene et al., 2014). Early modeling of the far-field tsunami was based on an assumed dislocation source the size of the aftershock area (cf. Okal & Hebert, 2007). The unmodified seafloor escarpments where a BSFZ emerges indicates active features that are shown in multibeam bathymetry (Flueh et al., 1994; Rathburn et al., 2009). A ~5 to 10-km-wide corridor of disturbed seafloor with anastomosing fault scarps and short winding en'echelon ridges indicates recent activity (Rathburn et al., 2009; von Huene et al., 2016).

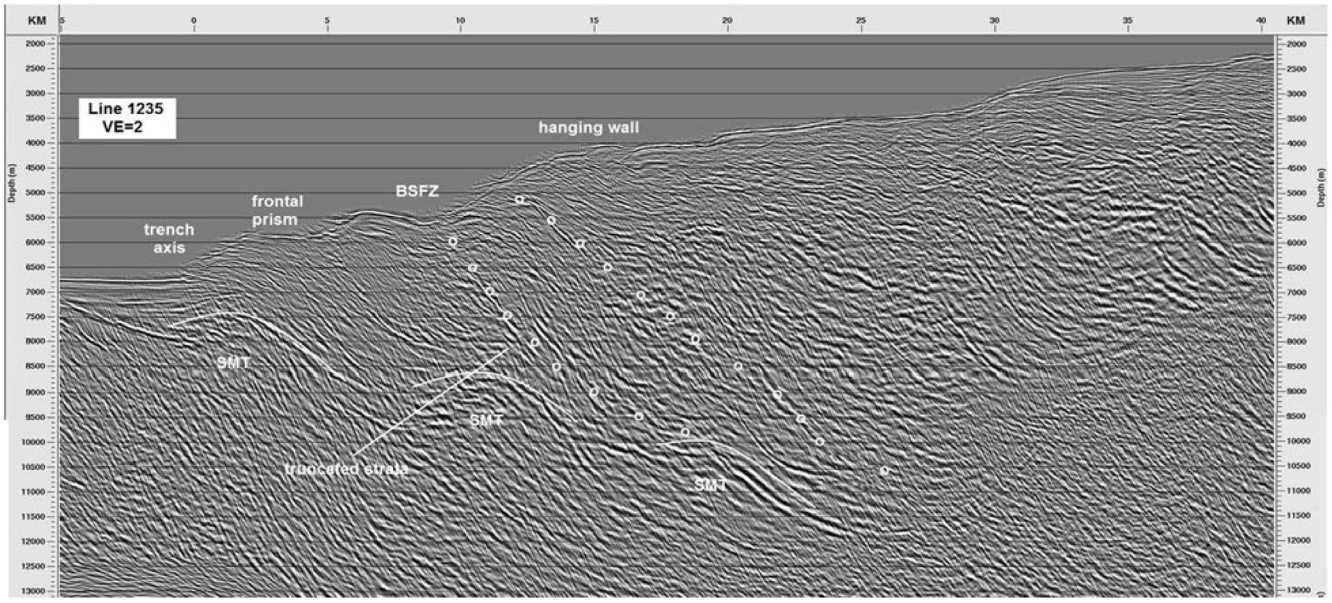

Figure 8. Depth section of line 1235 across the lower slope along the SW part of the Shumagin segment (after Miller et al., 2014). White dots approximate strong continuous reflections of a BSFZ shear zone. The BSFZ image quality is probably degraded by the seismic transect's angular crossing of bathymetry. BSFZ, backstop splay fault zone; SMT,reflectors indicating relief along the plate interface emphasized with white lines.

A seismic image across the Unimak segment, line 1237, (Figure 9) (von Huene et al., 2016) runs through an embayment from a subducted seamount in the accretionary prism. Therefore, a prism is missing and the BSFZ occurs farther landward. The BSFZ branches from the plate interface at a subducted seamount (Figure 2). The BSFZ ~1.4-km-thick damaged zone of diffuse reflectivity extends from the seafloor to 10-km depth (Figure 9) and is bordered by truncated strata. On the seafloor above the BSFZ, scarps and ridges are little modified by sedimentation or erosion (von Huene et al., 2016). On the landward side, a sediment cover deposited on the Oligo-Miocene unconformity continues to the shelf (Figure 2). The hanging wall of the BSFZ is cut by normal faults covered by unfaulted slope strata indicating extensional tectonism that is no longer active.

4. Plate Interface Relief in the Subduction Zone

Relief along the plate interface was either not resolved or recognized in 1980s processed legacy seismic images. At trench depths and beneath deformed frontal prism strata, resolution of relief with 2D seismic techniques is difficult (see supporting information S3). With advanced processing, however, relief at scales of hundreds of meters was resolved beneath the trench floor and in shallow regions of subduction zone (i.e., Figure 7). In two of the few seismic images extending across the entire trench, normal faults from plate bending or bend faults are imaged beneath the trench axis and the adjacent subduction zone (Figure 10). In the adjoining ocean basin, GLORIA images resolve low (~100 m) bend faults along outer trench slopes of the Semidi and Shumagin segments. Bend faults are reported locally in multibeam bathymetry along the Albatross segment (Krabbenhoeft et al., 2021; Reece et al., 2013). Bend faulting of the seaward slope and trench axis is resolved when resolution surpasses that afforded by standard seismic and regional bathymetric imaging.

In subduction zones, relief commonly appears higher than on the ocean basin seafloor of the incoming plate next to the trench axis (i.e., Figures 7 and 10). An indicator of increased fault displacement in the subduction zone is the uplift and depression of uniformly thick strata like pelagic sediment that was deposited on a flat seafloor (Figures 7 and 10). Pelagic sediment generally accumulates in parallel layers and is often of uniform thickness. Beneath the frontal prism, parallel strata on igneous crust draped over fault uplifts indicate growth of relief after subduction. In the Shumagin segment, an even seafloor adjacent to the trench

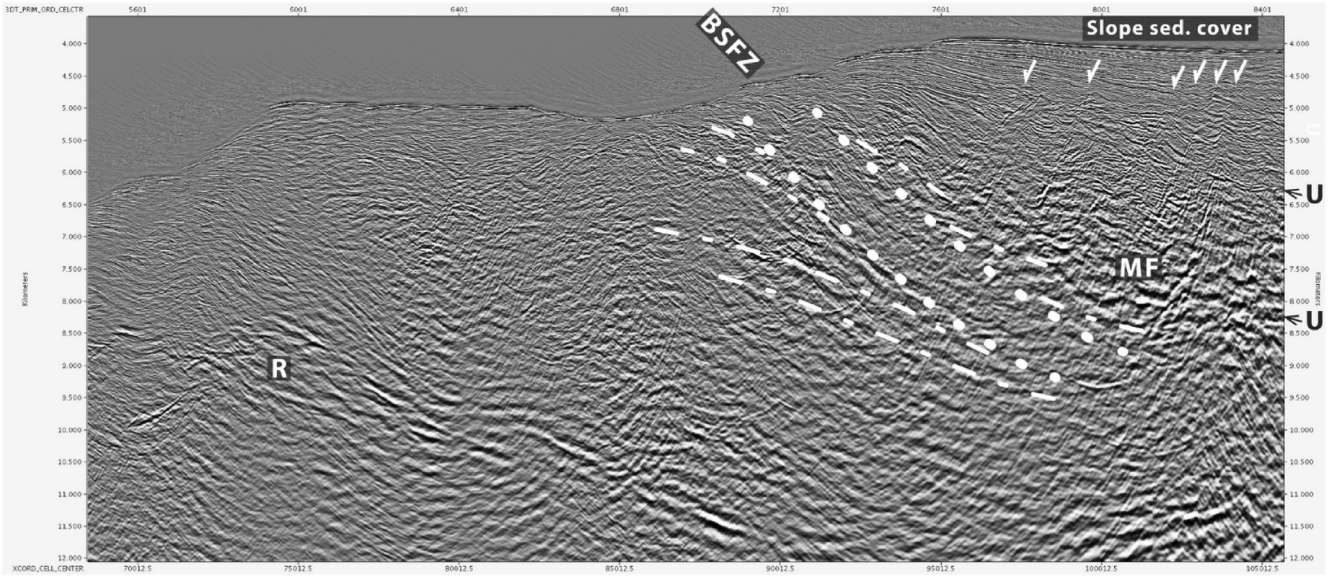

Figure 9. Unimak lower slope and backstop splay fault zone (BSFZ) imaged in line 1237. In the hanging wall, the Oligo-Miocene unconformity is displaced along seaward dipping normal faults that are not annotated to retain clarity. The BSFZ displaces the unconformity and is marked by truncated reflections (dashed lines). Enlargement helps see the truncated strata at the deformation front with a small pile of slide debris at its base. Landward tilted beds and the tilted terrace seafloor indicate hanging wall uplift from BSFZ displacement.

axis has some 200 m high fault scarps. Down the subduction zone, relief is ~ 2 km high (Figures 7 and 10). That lower plate relief is not an artifact of the velocity model (Figures S3-1 and S3-2).

Heightened normal fault relief in the subduction zone is easiest to explain as continued bend faulting. Subducted relief beneath the frontal prism is imaged in all segments of the Alaska margin. Deeper in the subduction zone the difference between a seamount and bend fault is obscured by attenuation. The difference between seamount relief that originated before subduction and that developing after entering the trench is its relation with the onlapped sediment. If strata abut rather than drape over the relief, it indicates an origin before subduction. Subduction zone relief is thought to modify plate interface coupling, is commonly associated with the BSFZ, and occurs in the subduction zone even where little incoming relief is mapped.

5. Fluid Vents

Seafloor vents become visible in enlarged GLORIA backscatter images (Figure 11). Vent features consist of circular craters on peaks or along the crests of mounds (Figures 11a and 11b). They top volcano-like features (Figure 11c) and locally, multiple vents are aligned along ridges with narrow summits (Figures 11B and 11c). Vents are commonly found on or near BSFZs in the Semidi and Shumagin segments and in the Albatross sector (Krabbenhoeft et al., 2021). Vents are also located in an area of disrupted morphology above the subducted Patton Murray and Semidi ridge intersection (Figure 1). Probable vents along the Shumagin segment BSFZ are found in the SW where morphology indicates relatively recent tectonism. Not all suspect vent features are resolved convincingly in GLORIA images and with better resolution vents and their sediment aprons would be clearer. Few suspect vents occur across the accreted prism and only a few suspect features are displayed up slope of the BSFZ. The resolution of GLORIA is insufficient to show small vents where near bottom surveys located seeps and vents (Suess et al., 1994).

Alaskan vents are similar to those investigated in greater detail along the Middle America margin. There, vents were studied with near bottom imaging systems, heat flow probes, and sampling that yielded fluid chemistry (Ranero et al., 2008; Sahling et al., 2008). The fluid chemistry indicates sources at or below the plate interface. Sediment volumes in the mounds indicates vigorous and variable flow rates as high as 300 cm/a. The Alaskan vent structures are consistent with seismic evidence of fluids concentrated along the

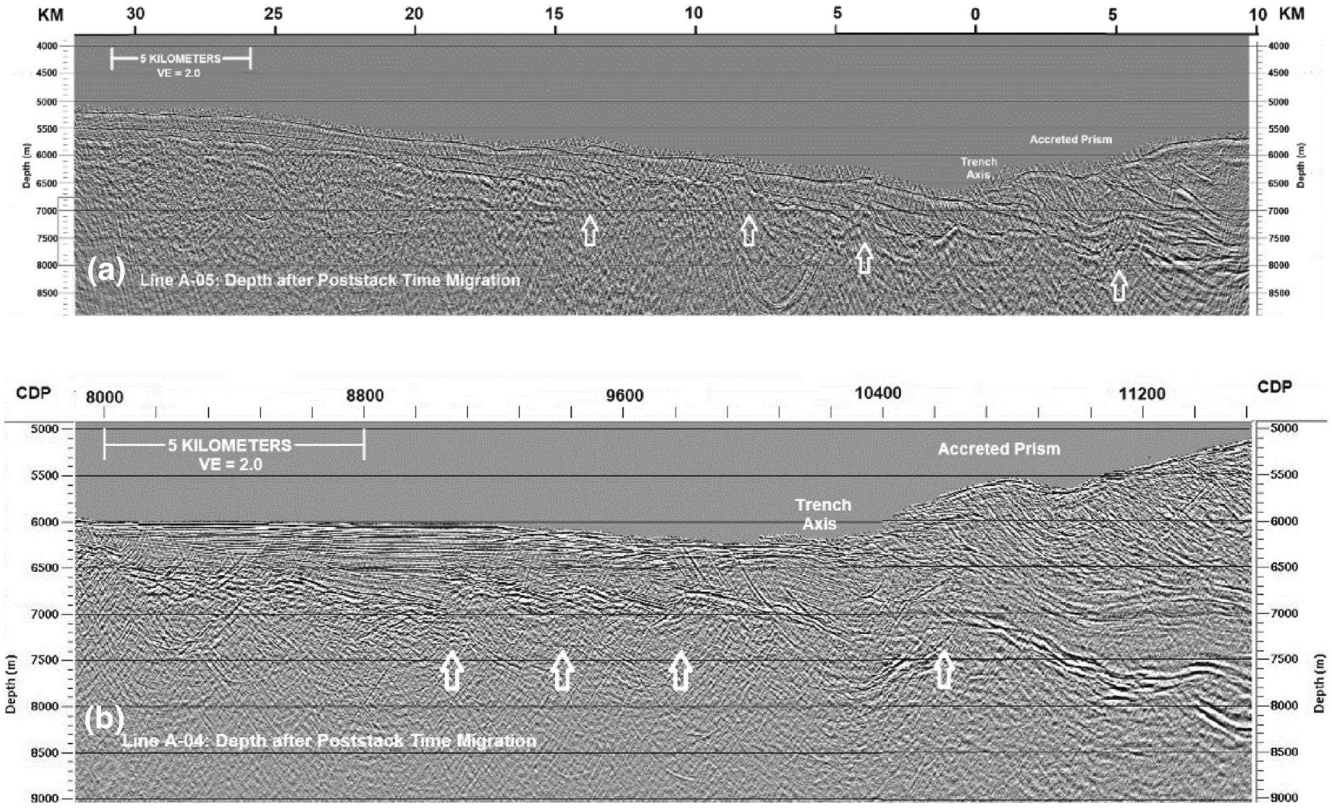

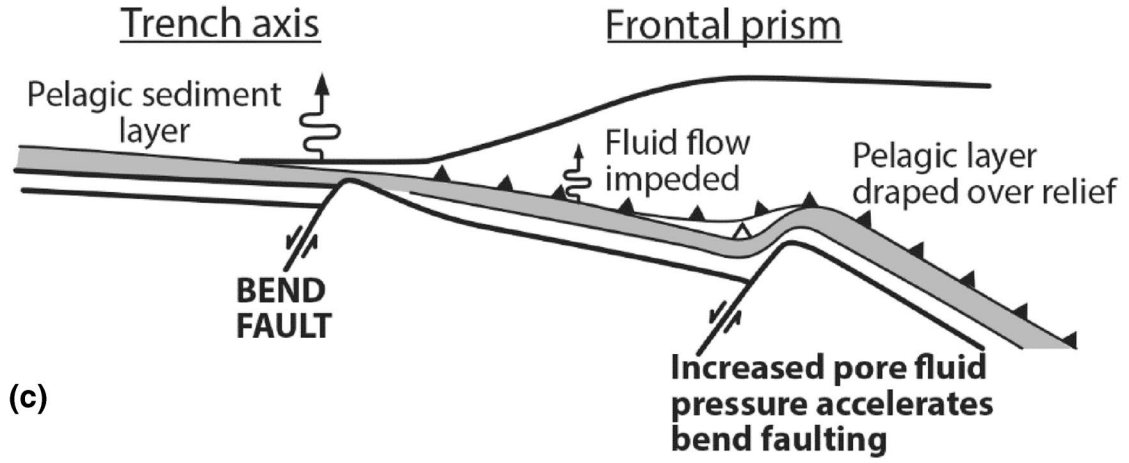

Figure 10. Seismic images of bend faults from the ocean basin to beneath the accreted prism (a) & (b) and a sketch of bend fault growth in the subduction zone (c). Faults displacing the igneous basement continue growing after subduction as long as lower plate bending continues. Strata of a uniformly thick pelagic sediment layer indicate continuing basement deformation when uplifted or depressed over highs and lows. Fluid pressure increases from loading of the prism and from coseismic fluid pressure spikes (Ma, 2012). Elevated fluid pressure reduces coupling along bend faults and relaxes resistance to fault displacement. As fault blocks grow to a critical height, the plate interface migrates upward to compensate for increased resistance from relief. This smooths the megathrust. Enlargement of the seismic images reveals fault structure more clearly.

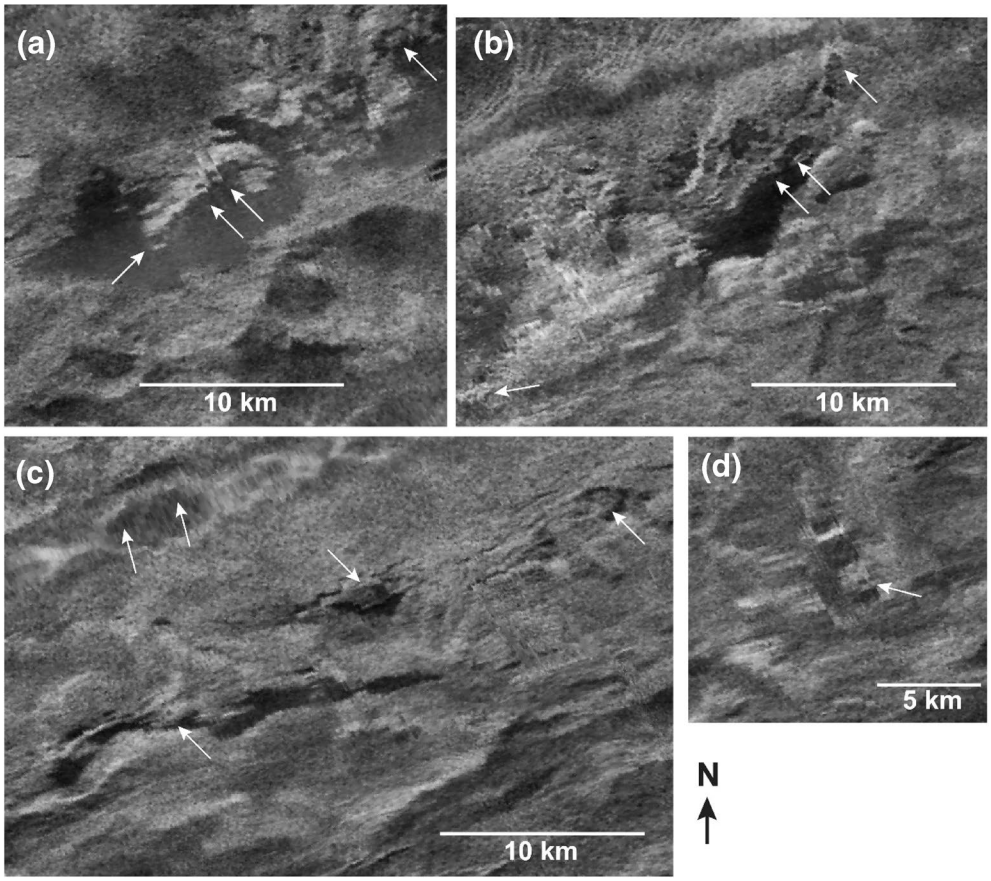

Figure 11. GLORIA images of vents on mounds at the NE end of the Semidi segment backstop splay fault zone (BSFZ) ridge and the subducted Patton-Murray ridge. Arrows point toward some of the vent areas recognized from circular features and enlargement helps resolve them. Bar scales are approximate. Location are shown with an orange V in Figure 1. The GLORIA signal backscatter frequency allows resolution of only relatively large vent features.

plate interface inferred from polarity and amplitude (Li et al., 2015). Many unresolved vents were postulated off Middle America (Ranero et al., 2008) despite instrumentation with greater resolution than GLORIA but limited ship time left many areas unsurveyed.

6. Discussion

6.1. Effects of Subducted Relief and Earthquake Asperities

Alaskan BSFZs are found in tectonic settings with a variety of subduction histories. The Neogene subduction history sketched previously provides some understanding of current morphology and structure unique to each aftershock segments of the Alaska Trench forearc. Kodiak-Bowie and Patton-Murray seamount chain subduction migrated NE along the Semidi and Kodiak segments as the Pacific and North American plates converged. A particularly disrupted area is the Albatross-Semidi boundary. Here transverse lineaments and embayments in the middle slope formed during past subduction of lower plate relief are preserved in consolidated rock of the margin framework. These vestiges of subducted relief stop at the BSFZ showing that the accreted prism postdates formation of mid-slope morphologic features. Abruptness of this contact zone indicates a missing rock record across the BSFZ. The deformation front is indented by young embayments without tracks up slope of the BSFZ. Disruption up slope of the BSFZ requires large lower plate features whereas disruption of the accreted prism shows subduction of smaller 1 km–2 km high currently subducting relief (Krabbenhoeft et al., 2021).

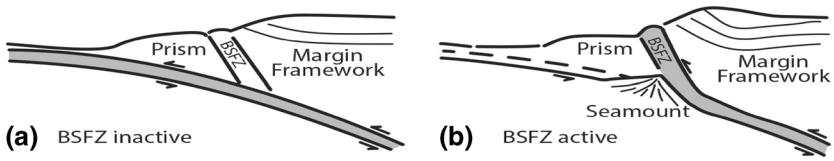

Figure 12. Sketches showing an inactive and an active BSFZ. (a) backstop splay fault zone (BSFZ) is inactive and the frontal prism remains with the upper plate. The plate interface reflections cut across the BSFZ damage zone. (b), An active BSFZ, where the frontal prism moves with the lower plate. Seamounts are commonly associated with activated BSFZs but are not necessary to divert slip up the splay fault. Dashed line is along a former top of the current inactive lower plate sediment layer.

We speculate that the 1964 earthquake asperity along the Kodiak Bowie trend at the Kodiak Island shore (Figure 1) (Ichinose et al., 2007) could be a large lower plate feature that entered the subduction zone at the Albatross-Semidi boundary. If the asperity's current location is backed-out along the plate convergence vector, it crosses the middle and upper slope disrupted morphology at the Albatross-Semidi boundary about 110 km away. With a current 6 mm/year. Convergence rate, that translates to 1.8 Myr as an age for the subduction of relief morphology in the Albatross area. In the Kenai sector to the north, the 1964 earthquake hypocenter is collocated with the 58° fracture zone magnetic anomaly. A boundary between the two asperities of the 1964 earthquake is also a convenient boundary between the different geologies of the NE and SW sectors.

The NE Kodiak asperity is located on the 58° fracture zone (Figure 3). Although its rough morphology is generally buried beneath Surveyor fan sediment its subducted lower plate relief is indicated by the embayment eroded into the deformation front (Figure 3 and S4-3). Across the shelf, its trend parallels bathymetric trends of Portlock Bank and Amatuli Trough rather than the margin's NE regional trend (Figure 1) so it extends to the Kenai Peninsula. Separation of the 1964 earthquake Kodiak asperities is consistent with division of the Kenai and Albatross rupture areas by a subducted extension of Kodiak-Bowie Ridge. An absence of clear geophysical markers across the inner shelf marking a ~25-km-deep subducted section of the ridge (Ye et al., 1997) could result from a stretch of weakly magnetic low relief like the one between Kodiak Seamount and the ridge seamounts about 180 km to the east (Figure 1). The inferred barrier was too weak to stop propagation of rupture during the 1964 earthquake.

The Kenai sector's middle continental slope of ridge and valley morphology differs from all others along the Alaska margin (Fruehn et al., 1999). At the SW end of the ridges morphology, the change from frontal prism to margin framework is inferred in cross section at a diffuse boundary in the EDGE seismic image (Figure 4). A change in seismic character at km 40 in Figure 4 is interpreted as the truncated margin framework's basement covered with mass wasting debris that was deformed by contractile interplate motion (Fruehn et al., 1999). Similar structure shaping Yakutat trailing flank in the current area of Yakutat terrane subduction are imaged in the TACT line (S4).

The middle slope ridges were probably those crossed during 1970s industry seismic reconnaissance and presented at meetings but controlled by industry confidentiality (Seely & Dickinson, 1977). These authors made a convincing case for an Alaska margin accretionary wedge from the trench to the shelf from proprietary industry data. However, with multibeam bathymetry and well-migrated seismic data, it is possible to see the difference between the frontal prism and mid slope ridges of dismembered margin framework rock.

Differences between the Albatross and Kenai sectors are comparable to the dissimilar character of seafloor relief that subducted beneath each of them. The Albatross sector was underthrust by the NW migrating Kodiak-Bowie Ridge, whereas the Kenai sector was shaped during subduction of the Yakutat terrane followed by collapse down its trailing flank illustrated in the TACT image (Figure S4-1). The TACT image shows how contractile deformation of the mass wasting material at the base of slope rapidly re-establishes a narrow frontal prism prior to receiving trench turbidites (supporting information S4). A similar process is observed behind the trailing flank of subducting seamounts at the Costa Rican margin. After destroying the frontal prism, seamounts tunnel beneath the margin framework elevating a steep slope that fails and produces mass wasting debris at its base to form a narrow frontal prism. Accretion of trench sediment follows to build a prism at critical taper (S4). Such tectonic junctures may illustrate the early development of some BSFZs.

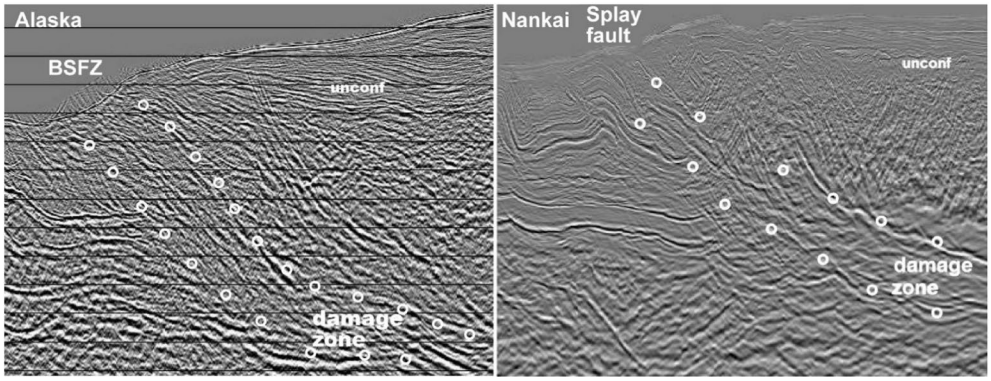

Figure 13. Comparison of Nankai and Alaska splay faults. The Nankai image is a section through the 3D volume (from Greg Moore) and the Alaska image is legacy line 217 (Figure 7). Dots approximate the splay fault damage zone boundaries. Notable similarities are strata on either side are cut locally and the incoming subducting trench sediment layer is terminated, the unconformity (unconf.) on hanging wall basement, seafloor rise above the splays, juncture of the fault damage zone forming the sediment layer on subducting igneous basement, and the change in seismic reflection pattern of the accreted prism and the hanging wall basement on either side of the splay fault.

The Albatross area's BSFZ ridge locally follows a broad embayment. Earthquake slip (Ichinose et al., 2007) peaked beneath this ridge and diminishes rapidly toward the trench axis (Figure 1). The high value of slip at the BSFZ may indicate a contribution to the tsunami during 1964 earthquake rupture (Krabbenhoeft et al., 2021).

In the Semidi area, the previously proposed BSFZ ridge origin from a subducted section of the Patton-Murray ridge (von Huene et al., 2015), failed to explain the change in ridge orientation. More likely, the basement ridge producing seafloor relief is the subducted Kula-Pacific ridge that appears cut on the NE by the Patton-Murray ridge. Kula-Pacific ridge formed a barrier to sediment transport from North America during earlier times. The complex intersection morphology could contain a pass that channeled sediment from North American for 10 Myr to form Zodiak fan (Stevenson & Embly, 1987, Figure 8). The fan's sediment feeder channels project toward this proposed intersection. Channeling sediment through an igneous barrier ridge explains how the fan apex remained in one position so long. The top of Zodiak fan's distinctive reflection at the division between subducted and accreted sediment ends at the ridge (Figures 5 and 6, plate interface sediment). In ALEUT 03 (Figure 6), the BSFZ follows the top of the ridge rather than the dashed lines inferred previously in two legacy seismic images (von Huene et al, 2015). This revision of inferred subducted structure removes problems with earlier reconstruction. This subducted ridge complex impedes the propagation of slip from the seismogenic zone and it forms part of the aftershock boundary between the Semidi and Kodiak rupture zones.

The minimal accretion in the Semidi embayment despite more than a Myr of convergence can be explained by a shift of the deformation front to the BSFZ and decreased accretion at the trench axis (Figure 12). Subducting relief first destroys the thin apex of the accreted prism until prism thickness exceeds the height of the seamount. The ridge then tunnels into the margin and its leading flank is a splay fault. The splay fault can be the main earthquake slip path to the seafloor and it becomes the principal deformation front minimizing accretion along the trench axis.

The Shumagin segment's proposed seismic creep (Fournier & Freymueller, 2007; Witter et al., 2014) indicates a different dynamic from all other segments as does its geology. Hudnut and Taber (1987) found discontinuity in subduction zone seismicity from records of a local seismometer network. A double Wadati-Benioff zone occurs in the SW whereas a single zone of earthquakes characterizes the NE. This discontinuity corresponds with a change in bathymetry and upper plate structure in seismic images. The SW slope morphology is rough indicating rock resistant to erosion whereas morphology in the NE is smoother [GEBCO_2014 Grid; von Huene et al., 2019, Figure S3]. The frontal prism is relatively narrow in the SW and the BSFZ juncture with the plate interface is shallower than in the NE (Figures 7 and 8). The sharp BSFZ ridge morphology in the SW is smoother and less linear in the NE. The upper slope buried Unimak ridge

also fades into a NE smoother seafloor. These upper plate and seismological differences divide this segment. In essence, the SW area is similar to the adjacent Unimak segment whereas the NE segment is similar to the Semidi segment but without the lower plate subducted ridge. Data interpreted as indicating creep came from investigations of the tectonically more active SW segment. On 22 July 2020, a M 7.8 earthquake was recorded beneath or near the zone of sector separation at 28-km depth, and aftershocks propagated SW to the aftershock boundary with the Unimak segment (earthquake.usgs.gov). No tsunami was reported. The potential for generation of a great tsunami in the Shumagin segment appears diminished by its divided structure.

Despite different tectonic histories of Alaska convergent margin earthquake segments, they all have a BSFZ. That ubiquitous occurrence indicates a fundamental convergent margin tectonic role.

6.2. Recognizing a BSFZ and Its Components

Awareness of BSFZ, adds a previously unrecognized tectonic element to assessments of Alaskan tsunami generation so they become important features to recognize. Alaskan BSFZs, first proposed in the Unimak segment, are now documented along backstops of the entire margin. BSFZs are more efficient tsunami generators than megathrust slip beneath the frontal prism (Lotto et al., 2019; Wendt et al., 2009). Splay fault slip in deep water is clearly a potent tsunami generator and a likely component of far-field tsunami generation. Shallow water on the shelf as along Middleton or Montague Islands thrust faults (Liberty et al., 2013; Plafker, 1972) are likely near-field tsunami generators.

Accreted prism faults and the BSFZ in seismic images above the seafloor multiple look alike. The multiple masks the plate interface that is commonly greater than 10-km deep beneath backstops. The BSFZ is most easily recognized from the continuation of splay fault damage zones into the subducting sediment layer that is commonly ≥10 km deep. Both the depth and the multiple make imaging with 2D seismic capabilities difficult.

The Alaskan backstop transition from prisms to margin framework rock is commonly clear in multibeam bathymetry integrated with carefully processed seismic images. Such recognition requires better resolution than most standard processed seismic images afford. Seismic resolution is commonly a function of good 2D structure. In addition, active BSFZs commonly have a laterally extensive seafloor step ±1 km high associated with ~2–6 km wide zones of fault scarps with some recent unmodified morphology. Truncated hanging wall strata indicate a missing rock volume and below the multiple, a mass flux can be observed with the BSFZ merger into the plate interface sediment layer (Figure 7). This continuity of BSFZ fault damage zones into the plate interface sediment layer is a vital distinguishing feature (Figure 12). The BSFZ commonly cuts across the subducting plate sediment layer beneath the prism either partially or fully (Figures 7 and 12b). BSFZ damage zones are nominally 1–5 km wide rather than the simple thrust faults in diagrams. The dynamic outcome reasoned from certain seismic images is that fragmented upper plate fault zone material transfers to the lower plate subducting sediment layer. The landward dipping reflections of the BSFZ are from fault gouge whereas those of the accreted prism are mostly trench sediment. The difference is difficult to resolve without high resolution in seismic records and detailed multibeam bathymetry. On hanging walls, the sediment cover and its underlying unconformity is deformed at the BSFZ rather than pinching out against the fault to indicate that sedimentation followed uplift. Identifying a combination of these features in merged bathymetric and seismic data is facilitated by a two dimensionality of structure and careful geophysical data processing.

The Shumagin juncture image is comparable to single line images through the Nankai margin 3D volume (Figure 13). Juncture of the BSFZ and subducting sediment is locally 4 km shallower than that of other segments positioning it above the seafloor multiple (Figure 7). This accounts for its clear juncture image. Its seafloor BSFZ escarpment is ~1-km high and well-defined in bathymetry, indicating recent activity consistent with the juncture. The splay fault-plate interface juncture along the Nankai 3-D seismic data shows submultiple variations of the juncture (G. F. Moore et al., 2007) and illustrates limitation of 2D seismic imaging of this 3D feature.

6.3. Interplate Rugosity

In models of Wendt et al. (2009), splay fault activation requires subducting relief (Figure 12). This is locally consistent with seamounts in our reprocessed images (Figures 5–8). However, in the decade later simulations of Lotto et al. (2019) subducting relief is not required. An absence of subducting relief is observed at the Nankai margin yet its scarps are up to 1-km high and indicate recent displacement. The difficulty of imaging subducting relief, especially at 10 km or more depths, is discussed in supporting information S3. Clear resolution of lower plate rugosity deep in subduction zones is exceptional without 3D seismic acquisition and a measure of its effects on fault coupling are not yet derived from observations. Another influence on fault coupling is fluid distribution (cf. Ranero et al., 2008). The shorter path to the seafloor of the BSFZ over the plate interface beneath the prism introduces another variable. So, the resistance to earthquake slip may not be much greater along the BSFZ than along the plate interface as shown by BSFZs that are active without much megathrust rugosity.

In the Shumagin and Semidi segments, igneous ocean crust entering the subduction zone is mostly smooth without bend fault displacement greater than ~500-m high beneath the trench axis turbidite, and yet in the subduction zone igneous crust has some ~2-km-high relief (Figure 10). An explanation is continued bend faulting after subduction facilitated by a constrained fluid escape as the frontal prism mass loads the zone. Elevated pressures spikes during earthquakes also increase prism yielding (Ma, 2012) and facilitate bend fault growth. Lower plate roughness from growing relief can increase interplate resistance to convergent plate forces until it exceeds that of the BSFZ. As long as the plate bends beneath the prism, the environment is favorable for growth of lower plate relief. As the bend faults grow, the plate boundary shifts upward to surmount a greater physical impediment and that effectively reduces plate interface roughness. Exposed bend faults extend laterally ~45 km and therefore their coupling patterns may extend laterally over a larger area than the 20 km diameter subducted seamounts we imaged. The complexity and size of earthquakes initiated by seamount asperities also appears limited by shape (Lallemand et al., 2018), as well as upper plate rigidity (Sallares & Ranero, 2019), and the amount of subduction zone roughness (Wang & Bilek, 2014). Lower plate roughness evolves as the plate subducts and the segment below the frontal prism is imaged better than that of the seismogenic zone. Seismogenic zone physical character inferred from incoming ocean basin morphology appears ambiguous but it is the most available visual global proxy.

Wang and Bilek (2011, 2014) hypothesize that plate interfaces with relief are prone to creep whereas smooth interfaces provide the environment for great and giant earthquakes. Seamount asperities produce earthquakes apparently no greater than M7. The 1964 M9.2 Alaska giant earthquake rupture area is in the list of smooth subduction interfaces. However, reprocessed seismic records show plate interface relief that develops after entry into the subduction zone and buried igneous crustal relief. How much rugosity will impede giant earthquakes?

The Gulf of Alaska seafloor, flanked by the Kodiak Bowie Ridge, the Patton-Murray ridge and the 58° Fracture zone, is smoothed in intervening areas by sediment of Surveyor and Zodiak fans. Surveyor Fan buries scattered seamounts 1–2 km high (Reece et al., 2013; Stevenson & Embley, 1987). Multibeam bathymetry along the Kenai frontal prism contains embayments from past subduction of seamounts and two currently impacting ones (Figure 3 and S4-3). The morphologically smooth seafloor entering the subduction zone continues down dip as a plate interface with basement relief 500 m high. In the Kenai subduction zone, relief is imaged in seven of eight seismic images beneath the lower slope. Subducted relief several km across in the SW Albatross sector is imaged with a grid of seismic lines that allow construction of 2.5D images (Krabbenhoeft et al., 2021). A rugose igneous ocean crust beneath the trench is covered by ~3 to ~5-km-thick sediment that modulates the plate interface megathrust configuration. Some relief originated prior to subduction and other relief developed in the subduction zone from continued lower plate bending. The latter type is generally 0.5–1.0 km high at the igneous crust below the plate interface fault zone and it may be smoothened along the plate interface. Subducting seamounts, in turn, are generally 2–3 km high on entry and remain prominent to the BSFZ. Plate interface morphology is rougher in the available geophysical data than inferred from the Gulf of Alaska seafloor between seamount chains and ridges.

In consideration of the Wang and Bilek study, the three 1964 earthquake asperities of Ichinose (2007) could have been M7 earthquakes had they nucleated separately. A minimum rupture area within the 4 m slip con-

tour was converted to earthquake magnitude with the scaling relations of Wells and Coppersmith (1994). The Prince William asperity nucleated an M8 plus earthquake, the Albatross asperity an M8 earthquake, and the 58° Fracture zone asperity a ~7.8 earthquake. Individually, the 1964 asperity earthquake magnitudes appear greater than expected for rough plate interfaces (Wang & Bilek, 2014).

Morphology of the incoming Gulf of Alaska ocean floor may be the best available proxy for morphology in the seismogenic zone but it has severe limitations. Resolution with 2D seismic techniques, even with the powerful seismic system of RV Langseth, leaves obscured images of plate interface roughness downdip of the BSFZ (e.g., Bécel et al., 2017). Ocean basement roughness up-dip from BSFZs probably increases interplate coupling beneath the frontal prism but great and giant earthquakes commonly nucleate downdip of the BSFZ and well beyond most 2D imaging. The BSFZ transition is notable since it involves a physical property change and a lateral increase in seismic P-wave velocities. It is located near the updip end of the seismogenic zone (S. L. Bilek and Lay, 1999, 2018]. The magnitude of lower plate rugosity and plate interface relief apparently influence coupling beneath the frontal prism to direct slip up the BSFZ but its relation to the source of tsunami earthquakes in the seismogenic zone is speculative. The link between structure and seismic behavior related to lower plate relief is based largely on inference and reasoning as Wang and Bilek (2014).

Imaging asperities in the seismogenic zone is improved with 3D seismic technology and vertical seismic profiles. A seamount asperity for the 1990 7.0 earthquake off Costa Rica (Husen et al., 2002) was revealed with tomography but imaging its morphology or the surrounding strata requires a much denser data set. Observations of large subducted seamounts are probably underreported because rough sloping volcanic surfaces at depths greater than ~5 km are 3D objects difficult to image with 2D seismic techniques (see supporting information S3). Up dip of the seismogenic zone, some relief is locally resolved with 2D reflection techniques but we deduced relief more than 2 km high from deflected and terminated strata (Figures 2 and 7).

Comprehensive studies of tsunami earthquakes related to splay fault zones other than the Nankai Trough are few. The truncated rocks adjacent to the BSFZ show the source of its dismembered material in damage zones. Damage zones fault rock sampled off New Zealand, consists of Breccias with 40% porosity (Fagereng et al., 2019). The permeability of fault damaged rock probably make it a conduit for the fluid migration such as that associated with seafloor vents along the Alaska margin (Figure 11). Damage zone rocks have reduced elastic moduli, cohesion, and yield strength, which can promote attenuation and reduced wave propagation during ruptures as occurs in tsunami earthquakes. An association of BSFZs and tsunami earthquakes is suggested by the 1946 hypocenter beneath a BSFZ's bathymetry in the Unimak segment. Fukao (1979) suggested that soft sediment of an accreted prism slows rupture, which was echoed by others (e.g., Lopez & Okal, 2006). The physical properties of "soft" are indicated by Alaskan seismic V_p velocities. Accreted trench turbidites have velocities around 1.6 km/s in DSDP trench sediment cores, and 1.7 km/s in sonobuoy refraction data (Kulm et al., 1973; Ye et al., 1997). Wide-angle seismic velocities of 3.0–3.8 km/s are measured in accreted sediment ~10 km from the Kodiak segment deformation front (Krabbenhoeft et al., 2021; Ye et al., 1997). Such prism velocities are usually associated with consolidated rather than "soft" trench sediment.

Another mechanism for slowing rupture is proposed by Ma (2012). He modeled dynamic deformation of the accreted prism assuming a V_s speed of 3.4 km/s and near-critical stresses for Coulomb failure of the wedge. His results indicate that dynamic pore pressure changes can lead to widespread yielding of the prism, which reduces rupture speed and lengthens rupture duration. Off-fault yielding (Ma, 2012) of sediment such as that drill-cored in the Hikurangi margin splay fault (Fagereng et al., 2019) slows rupture propagation. Other modelers have found that a very rugose plate interface fault can retard slip and induce failure within the wedge (cf. Dieterich & Deborah, 2009). Wide damage zones of fragmented rock in BSFZs, might slow fault propagation (Ma, 2012). In the Unimak segment, from where the defining tsunami earthquake was recorded, the 3 to 5-km-wide BSFZ fault zone could distribute fault slip over a wide zone (von Huene et al., 2016). However, measuring velocities and deriving physical properties of a 25° dipping low velocity layer is a technical challenge.

The BSFZ damage zone and a rough lower plate are two suspected seismological velocity-reducing features added to considerations of possible processes in frontal wedges promoting tsunami earthquakes. The structural complexity of convergent margins allows multiple velocity reducing processes to act concurrently.

7. Summary and Conclusions

Tectonic structure crossing the regional trend occurs along limits of the aftershocks following great and giant earthquakes. They are apparent in three boundaries that have adequate geophysical data. Morphology indicates possible upper plate transverse structure at the other two. The giant 1964 earthquake transgressed the Yakutat-Kodiak segment boundary and ruptured two large Kodiak sectors. Anecdotal information and sediment paleoseismology suggests that the 1788 earthquake may have crossed boundaries. Nonetheless, boundaries indicate the length of segments that could generate future tsunamis.

Alaska tsunami hazards were widely recognized after the 1946 Unimak earthquake's Pacific wide traverse. It was a tsunami earthquake with a hypocenter located beneath seafloor ridges of a 3 to 5-km-wide BSFZ. Modeling studies indicate a high efficiency of splay faults as tsunamis generators (Lotto et al., 2019 and references therein). BSFZs run along all Alaska Trench great and giant earthquake aftershock areas. In the absence of sample analysis, activity is inferred from the character of multibeam morphology above the BSFZ. Multibeam bathymetry also resolves many subducted seamount entry embayments into the Alaskan accretionary prism. Subducted relief down to 10 km depths is revealed in reprocessed legacy seismic images even where the adjacent incoming ocean basin seafloor is relatively smooth. Bend faults continue growing beneath the frontal prism probably as long as lower plate bending continues. At or near BSFZs, seafloor fluid vent structures indicate elevated fluid pressure. Locally, subducted relief and the BSFZ occur together, and their overlying seafloor fault scarps indicate recent displacement. We reason that plate interface relief can increase megathrust coupling enough to divert earthquake slip up the shorter BSFZ locally rather than continuing to the trench axis. BSFZ activation is also indicated without a triggering seamount.

When active, BSFZs introduce fault gouge into the sediment layer on the subducting lower plate (cf. Figure 7). Active BSFZs are erosive, contributing fragmented upper plate rock to the subducting lower plate sediment layer thereby contributing to plate interface rock heterogeneity.

Alaskan BSFZs are a core of the transition between the continental margin basement framework and the compliant accreted prism. The framework and prism are of dissimilar age, history, and physical properties as is apparent from structure and seismic properties. The upper plate horizontal V_p gradient increases across the transition. Modeling illustrates BSFZ's large tsunami generating potential. Multibeam bathymetry of active BSFZ faulting shows a colocation of BSFZs and seismogenic zone updip limits. In the Unimak segment, the 1946 epicenter proximity to the BSFZ allows for possible splay involvement. In the Albatross segment, a modeled slip maximum (Ichinose et al., 2007) collocates with the area's BSFZ. Core samples of vent mound sediment can reveal periods of heightened fluid expulsion that could be linked with great and giant earthquake records.

Data Availability Statement

Original seismic data are archived at: Line 102wg81: https://walrus.wr.usgs.gov/NAMSS/survey/l-8-81-wg/.Line 217wg82: https://walrus.wr.usgs.gov/namss/survey/l-12-82-wg/.Hinchinbrook and Tact lines: https://walrus.wr.usgs.gov/namss/survey/g-01-88-eg/.Ewing Lines 1235 and 1237: https://doi.org/10.3133/ofr20141024.Edge Line: https://www.marine-geo.org/tools/search/Files.php?data_set_uid=28283. Line ALEUT-03, A-04 A-05: https://www.marine-geo.org/tools/search/Files.php?data_set_uid=17810. In Figure 1, multibeam bathymetry, the extent and some annotation are modified from Krabbenhoeft et al., (2021). Regional multibeam bathymetric data (Flueh & von Huene, 1994; Rathburn et al., 2009; Shillington et al., 2015; Suess, 1994) were gridded at 150 m × 150 m using the WGS84 horizontal datum and a Gaussian weighted mean filter gridding algorithm. In regions without multibeam coverage, the latest release of the GEBCO 30 arc-second global grid of elevations, the GEBCO_2014 Grid, were integrated with the processed multibeam bathymetry.

Acknowledgments
Discussions with Dirk Klaeschen, David Scholl, and Eric Geist helped shape this report. Jim Dieterich reviewed and contributed to the seismological aspects. Greg Moore kindly contributed an image from the Nankai 3D volume. USGS reviews by Rob Witter, Daniel Scheirer, and four journal reviewers were instrumental in reshaping our original manuscript. RvH acknowledges encouragement and support for travel from the USGS emeritus scientist fund administered by Ruth Harris and Walter Mooney.

References

Bassett, D., & Watts, A. B. (2015). Gravity anomalies, crustal structure, and seismicity at subduction zones: 2. Interrelationships between fore-arc structure and seismogenic behavior. *Geochemistry, Geophysics, Geosystems*, *16*, 1541–1576. https://doi.org/10.1002/2014GC005685

Bécel, A., Shillington, D. J., Delescluse, M., Nedimović, M. R., Abers, G. A., Saffer, D. M., et al. (2017). Tsunamigenic structures in a creeping section of the Alaska subduction zone. *Nature Geoscience*, *24*. https://doi.org/10.1038/NGEO2990

Bilek, S. L., & Lay, T. (1999). Rigidity variations with depth along interplate megathrust faults in subduction zones. *Nature*, *400*, 443–446.

Bilek, S. L., & Lay, T.. (2018). Subduction zone megathrust earthquakes. *Geosphere*, *14*(4), 1–33, https://doi.org/10.1130/GES01608.1

Briggs, R. W., Engelhart, S. E., Nelson, A. R., Dura, T., Kemp, A. C., Haeussler, P. J., et al. (2014). Uplift and subsidence reveal a nonpersistent megathrust rupture boundary (Sitkinak Island, Alaska). *Geophysical Research Letters*. https://doi.org/10.1002/(ISSN)1944-8007

Brocher, T. M., Fuis, G. S., Fisher, M. A., Plafker, G., Taber, J. J., & Christensen, N. I. (1994). Mapping the megathrust beneath the Northern Gulf of Alaska using wide-angle seismic data. *Journal of Geophysical Research*, *99*(B6), 11663–11885.

Bruns, T. R., & Schwab, W. C. (1983). Structure maps and seismic stratigraphy of the Yakataga segment of the northern Gulf of Alaska: U.S. Geological survey Miscellaneous field studies map MF1424, 4sheets, 20p., scale 1:250,000.

Bruns, T. R., von Huene, R., & Culotta, R. C., (1987). Geology and petroleum potential of the Shumagin margin, Alaska. In D. W. Scholl, A. Grantz, J. G. Vedder (Eds.), Geology and resource potential of the continental margin of western North America and adjacent ocean basins—Beaufort Sea to Baja California: Houston, Texas, Circum-Pacific Council for Energy and Mineral Resources, Earth Science Series, (Vol. 6, pp. 157–190).

Byrne, D. E., Davis, D. M., & Sykes, L. R. (1988). Loci and maximum size of thrust earthquakes and the mechanics of the shallow region of subduction zones. *Tectonics*, *7*, 833–844. https://doi.org/10.1029/TC007i004p00833

Clift, P. D., & Vannucchi, P. (2004). Controls on tectonic accretion versus erosion in subduction zones: Implications for the origin and recycling of the continental crust. *Review of Geophysics*, *42*, 2003RG000127. https://doi.org/10.1029/2003RG000127

Dieterich, J. H., & Deborah, E. S. (2009). Nonplanar faults: Mechanics of slip and off-fault damage, *Pure and Applied Geophysics*, *166*, 1799–1815.0033–4553/09/101799–17. doi https://doi.org/10.1007/s00024-009-0517-y

Fagereng, A., Savage, H. M., Morgan, J. K., Wang, M., Meneghini, F., Barnes, P.M., et al., (2019). Mixed deformation styles observed on a shallow subduction thrust, Hikurangi margin, New Zealand, *Geology*, *47*, 1–5. https://doi.org/10.1130/G46367.1

Fisher, M. A., & Holmes, M. L. (1980). Large-scale structure of deep strata beneath Kodiak shelf, Alaska. *Geological Society of America Bulletin, Part I*, *91*, 218–224.

Flueh, E. R., & von Huene, R. (1994). FS Sonne Fahrtbericht SO96 Kodiak Seis, Hong Kong – Kodiak – Kodiak, 09.06. – 26.07.1994; Geomar interner Fahrtbericht.

Fournier, T. J., & Freymueller, J. T. (2007). Transition from locked to creeping subduction in the Shumagin region, Alaska. *Geophysical Research Letters*, *34*, L06303.

Fruehn, J., & von Huene, R. (1999). Accretion in the wake of terrane collision: The Neogene accretionary wedge off Kenai Peninsula, Alaska. *Tectonics*, *18*(2), 263–277.

Fryer, G. J., & Tryon, M. D. (2005). Great earthquakes, gigantic landslides, and the continuing enigma of the April Fool's tsunami of 1946. *EOS Transactions AGU86*, *52*, T11A–T0355.

Fukao, Y. (1979). Tsunami earthquakes and subduction processes near deep-sea trenches. *Journal of Geophysical Research*, *84*, 2303–2314.

GEBCO 2019 Grid, (2019). GEBCO Compilation Group. https://doi.org/10.5285/836f016a-33be-6ddc-e053-6c86abc0788e

Holbrook, W. S., Lizarralde, D., McGeary, S., Bangs, N., & Diebold, J. (1999). Structure and composition of the Aleutian island arc and implications for continental crustal growth. *Geology*, *27*, 31–34. https://doi.org/10.1130/0091-7613(1999)027<0031:SACOTA>2.3.CO;2

Hudnut, K. W., & Taber, J. J. (1987). Transition from double to single Wadati-Benioff seismic zone in the Shumagin Islands, Alaska, Geophysical. *Research Letters*, *18*, 143–146.

Husen, S., Quintero, R., & Kissling, E. (2002). Tomographic evidence for a subducted seamount beneath the gulf of Nicoya, Costa Rica, the cause of the 1990 Mw = 7.0 Gulf of Nicoya earthquake. *Geophysical Research Letters*, *29*(8). https://doi.org/10.1029/2001GL014045

Ichinose, G., Somerville, P., Thio, H. K., Graves, R., & O'Connell, D. (2007). Rupture process of the 1964 Prince William Sound, Alaska, earthquake from the combined inversion of seismic, tsunami, and geodetic data. *Journal of Geophysical Research*, *112*, B07306. https://doi.org/10.1029/2006JB004728

Kirby, S., Scholl, D., von Huene, R., & Wells, R. (2013). Alaska earthquake source for the SAFRR tsunami scenario, Chapter B, studies by the U.S. Geological Survey in Alaska, 2011, history of earthquakes and tsunamis along the Eastern Aleutian-Alaska Megathrust, with Implications for tsunami hazards in the California continental Borderland Chapter B in the SAFRR(science Application for Risk Reduction) tsunami scenario.

Krabbenhoeft, A., von Huene, R., Miller, J. J., & Klaeschen, D. (2021). Subducting oceanic basement roughness impacts on upper plate tectonic structure and a backstop splay fault zone activated in the southern Kodiak aftershock region of the Mw 9.2, 1964 megathrust rupture, Alaska, Geospheres, Themed Issue. Subduction Top to Bottom 2(ST2B-2). https://doi.org/10.1130/GES02275.1

Krabbenhoeft, A., von Huene, R., Miller, J., Lange, D., & Vera, F. (2018). Strike-slip 23 January 2018 Mw 7.9 Gulf of Alaska rare interplate earthquake: Complex rupture of a fracture zone system. *Scientific Reports*, *8*, 13706. https://doi.org/10.1038/s41598-018-32071-4

Kulm, L. D., von Huene, R., Duncan, J. R., Ingle, J. C., Kling, S. A., Musich, L. F., et al. (1973). Initial Reports of the deep Sea drilling project (Vol. 18, p. 411). Washington, DC: US Government Printing Office.

Lallemand, S., Peyret, M., van Rijsingen, E., Arcay, D., & Heuret, A. (2018). Roughness characteristics of oceanic seafloor prior to subduction in relation to the seismogenic potential of subduction zones. *Geochemistry, Geophysics, Geosystems*, *19*(7), 2121–2146. https://doi.org/10.1029/2018GC007434

Lewis, K. B., Ladd, J. W., & Bruns, T. R. (1988). Structural development of an accretionary prism by thrust and strike-slip faulting: Shumagin region, Aleutian Trench. *Geological Society of America Bulletin*, *100*(5), 767–782.

Liberty, L. M., Shaun, P. F., Peter, J. H., Thomas, L. P., & Andrew, P. (2013). Megathrust splay faults at the focus of the Prince William Sound asperity, Alaska. *Journal of Geophysical Research: Solid Earth*, *118*(10).

Li, J., Shillington Donna, J., Becel, A., Nedimovic, M. R., Webb, S. C., Saffer, D. M., et al. (2015). Downdip variations in seismic reflection character, implications for fault structure and seismogenic behavior in the Alaska subduction zone. *Journal of Geophysical Research*. *120*, 7883–7904. https://doi.org/10.1002/2015JB012338

Lopez, A. M. & Okal, E. A. (2006). A seismological reassessment of the source of the 1946 Aleutian "tsunami" earthquake. *Geophysical Journal International*, *165–3*, 835–849.

Lotto, G. C., Tamara, N. J., & Dunham, E. M. (2019). Fully coupled simulations of megathrust earthquakes and tsunamis in the Japan trench, Nankai Trough, and Cascadia subduction zone. *Pure and Applied Geophysics*, *176*, 4009–4041. https://doi.org/10.1007/s00024-018-1990-y

Ma, S. (2012). A self-consistent mechanism for slow dynamic deformation and tsunami generation for earthquakes in the shallow subduction zone. *Geophysical Research Letters*, *39*, L11310. https://doi.org/10.1029/2012GL051854

Miller, J. J., von Huene, R., & Ryan, H. F. (2014). The 1946 Unimak Tsunami Earthquake Area- Revised tectonic structure in reprocessed seismic images and a suspect near field tsunami source. *U.S. Geological Survey Open File Report*, 2014–1024. https://doi.org/10.3133/ofr20141024

Moore, J. C. (1972). Uplifted trench sediments: South-western Alaska-Bering Shelf edge. *Science*, 17559–17577.

Moore, J. C., Diebold, J., Fisher, M. A., Sample, J., Brocher, T., & Talwan, M., et al. (1991). EDGE deep seismic reflection transect of the eastern Aleutian arc trench layered lower crust reveals underplating and continental growth. *Geology*, *9*, 420–424.

Moore, G. F., Bangs, N. L., Taira, A., Kuramoto, S., Pangborn, E., & Tobin, H. J. (2007). Three-dimensional splay fault geometry and implications for tsunami generation. *Science*, *318*, 1128–1131. https://doi.org/10.1126/science.1147195

Moore, J. C., Byrne, T., Plumley, P. W., Reid, M., Gibbons, H., & Coe, R. S. (1983). Paleogene evolution of the Kodiak Islands, Alaska: Consequences of a ridge-trench interaction in a more southerly latitude. *Tectonics*, *2*(3), 265–293.

Nelson, A. R., Briggs, R. W., Dura, T., Engelhart, S. E., Gelfenbaum, G., Bradley, L.-A., et al. (2015). Tsunami recurrence in the eastern Alaska-Aleutian arc: A holocene stratigraphic record from Chirikof Island, Alaska. *Geosphere*, *11*, 1172–1203. https://doi.org/10.1130/GES01108.1

Okal, E. A., & Hebert, H. (2007). Far-field simulation of the 1946 Aleutian tsunami. *Geophysical Journal International*, *169*, 1229–1238. https://doi.org/10.1111/j.1365246X.2007.03375

Okal, E. A., Synolakis, C. E., Fryer, G. J., Heinrich, P., Borrero, J. C., Ruscher, C., et al. (2002). A field survey of the 1946 Aleutian tsunami in the far field. *Seismological Research Letters*, *73*, 490–503.

Plafker, G. (1972). Alaskan earthquake of 1964 and Chilean earthquake of 1960: Implications for arc tectonics. *Journal of Geophysical Research*, *77*, 901–925.

Ranero, C. R, Grevemeyer, I., Sahling, H., Barchkhausen, U., Hensen, C., & Wallmann, K. (2008). Hydrogeological system of erosional convergent margins and its influence on tectonics and interplate seismogenesis. *Geochemistry, Geophysics, Geosystems*, *9*, Q03S04. https://doi.org/10.1029/2007GC001679

Rathburn, A. E., Levin, L. A., Tryon, M., Gieskes, J. M., Martin, J. B., Perez, M. E., et al. (2009). Geological and biological heterogeneity of the Aleutian margin (1965-4822m). *Progress in Oceanography*, *80*, 22–50.

Reece Robert, S., Sean, P., Gulick, S., Horton, B. K., Christeson, G. L., & Worthington, L. L. (2013). Surveyor fan and channel system. *Gulf of Alaska Geosphere*, *7*(20114), 830–844. https://doi.org/10.1130/GES00654.1

Ruppert, N., Lees, J., & Kozyreva, N. (2007). *Seismicity, earthquakes and structure along the Alaska-Aleutian and Kamchatka-Kurile subduction zones: A review*, Washington DC: American Geophysical Union Geophysical Monograph Series. https://doi.org/10.1029/172GM12

Ryan, H. F., von Huene, R., Wells, R. E., Scholl, D. W., Stephen, K., & Draut, A. E. (2013). Studies by the U.S. Geological survey in Alaska, 2011, history of earthquakes and tsunamis along the eastern Aleutian-Alaska megathrust, with Implications for tsunami hazards in the California continental Borderland Chapter B in the SAFRR (science Application for Risk Reduction) tsunami scenario.

Sahling, H., Masson, D. G., Ranero, C. R., Hühnerbach, V., Weinrebe, W., Klaucke, I., et al. (2008). Fluid seepage at the continental margin offshore Costa Rica and southern Nicaragua. *Geochemistry, Geophysics, Geosystems*, *9*, Q05S05. https://doi.org/10.1029/2008GC001978

Sallarès, V., & Ranero, C. R. (2019). Upper-plate rigidity determines depth-varying rupture behaviour of megathrust earthquakes. *Nature*, *576*, 96–101. https://doi.org/10.1038/s41586-019-1784-0

Scholl, D. W. (2007). Viewing the tectonic evolution of the Kamchatka-Aleutian (KAT) connection with an Alaska crustal extrusion perspective. In J. Eichelberger, et al., Volcanism and subduction: The Kamchatka Region, Geophysical Monograph Series (Vol. 172). Canadian Journal of Earth Sciences. https://doi.org/10.1029/172GM03

Schwab, W. C., Bruns, T. R., & von Huene, R. (1980). *Maps showing structural interpretation of magnetic lineaments in the northern Gulf of Alaska.*. Reston, VA: U.S. Geological Survey. Schwab and Bruns, Magnetic Map, northern Gulf of Alaska, 1;500,000. Map MF 1054.

Seely, D. R. (1977). The significance of landward vergence and oblique structural trends on trench inner slopes. In M. Talwani (Ed.), *Island arcs, deep sea trenches and back-arc basins*. Washington, DC: AGU.

Seely, D. R. & Dickinson, W. B. (1977). Stratigraphy and structure of compressional margins. AAPG Continuing Education Short Note, series No. 5, pp. C1–C23.

Shennan, I., Barlow, N., Carver, G., Davies, F. (2014). Great tsunamigenic earthquakes during the past 1000 yr. on the Alaska megathrust. *Geology*, *42*(8), pp. 687–690.

Shillington, D. J., Becel, A., Nedimovic, M. R., Webb, S. C., Kuehn, H., Abers, G. A., et al. (2015). Link between plate fabric, hydration and subduction zone seismicity in Alaska. *Nature Geoscience*, *8*, 961–964. https://doi.org/10.1038/ngeo02586

Stevenson, A. J., & Embley, R. (1987). Deep sea fan bodies, terrigenous turbidite sedimentation, and petroleum geology, Gulf of Alaska. In D. W. Scholl, A. Grantz, & J. G. Vedder (Eds.), *Geology and resource. Potential of the continental margin of western N. America and adjacent ocean basins - Beaufort Sea to Baja California* (pp. 503–522) American Association Petroleum Geology.

Stock, J., & Molnar, P. (1988). Uncertainties and implications of the Late Cretaceous and Tertiary position of North America relative to the Farallon, Kula, and Pacific plates. *Tectonics*, *7*, 1339–1384. https://doi.org/10.1029/TC007i006p01339

Suess, E. (1994). FS Sonne Fahrtbericht SO97 Kodiak vent, Kodiak – Dutch Harbour – Tokio - Singapur, 27.07. – 19.09.1994; GEOMAR-Report 29. Kiel: GEOMAR Forschungszentrum für marine Geowissenschaften. https://doi.org/10.3289/GEOMAR_REP_29_1994

Sykes, L. R. (1971). Aftershock zones of great earthquakes, seismicity gaps, and earthquake prediction for Alaska and the Aleutians. *Journal of Geophysical Research*, *76*, 8021–8041.

Sykes, L. R., Kisslinger, J. B., House, L., Davies, J. N., & Jacob, K. H. (1980). Rupture zones of great earthquakes in the Alaska-Aleutian arc, 1784 to 1980. *Science*, *210*, 1343–1345, https://doi.org/10.1126/science.210.4476.1343

Turner, R. F., Lynch, M. B., Conner, T. A., Halin, P. J., Hoose, P. I., Martin, G. C., et al. (1987). Geological and operational summary, Kodiak Shelf stratigraphic test wells, western Gulf of Alaska U.S. Department of the Interior Minerals Management Service OCS Report MMS 87–0109.

von Huene, R., Klaeschen, D., Gutscher, M.-A., & Fruehn, J. (1998). Mass and fluid flux during accretion at the Alaska Margin. *The Geological Society of America Bulletin*, *110*(4), 468–482.

von Huene, R., Kirby, S., Miller, J., & Dartnell, P. (2014). The destructive 1946 Unimak near-field tsunami: New evidence for a submarine slide source from reprocessed marine geophysical data. *Geophysical Research Letters*, *41*, 6811–6818. https://doi.org/10.1002/2014GL061759

von Huene, R., Miller, J. J., & Dartnell, P. (2015). A possible transoceanic tsunami directed toward the U.S. west coast from the Semidi segment, Alaska convergent margin. *Geochemistry, Geophysics, Geosystems*, *17*, 645–659. https://doi.org/10.1002/2015GC006147

von Huene, R., Miller, J. J., Klaeschen, D., & Dartnell, P. (2016). A possible source mechanism of the 1946 Unimak Alaska far-field tsunami: Uplift of the mid-slope terrace above a splay fault zone. *Pure and Applied Geophysics*, *173*, 4189–4201. https://doi.org/10.1007/s00024-016-1393-x

von Huene, R., Miller, J. J., & Krabbenhoeft, A. (2019). The Shumagin seismic gap structure and associated tsunami hazards, Alaska convergent margin. *Geosphere*, *15*(2), 1–18. https://doi.org/10.1130/GES01657.1

von Huene, R., Miller, J., & Weinrebe, W. (2012). Subducting plate geology in three great earth-quake ruptures on the western Alaska margin, Kodiak to Unimak [online]. *Geosphere*, *8*(3). https://doi.org/10.1130/GES00715

Wang, K., & Bilek, S. L. (2014). Fault creep caused by subduction of rough seafloor relief. *Tectonophysics*, *610*, 1–24. https://doi.org/10.1016/j.tecto.2013.11.024

Wells, D. L., & Coppersmith, K. J. (1994). New Empirical Relationships among Magnitude, Rupture Length, Rupture Width, Rupture Area, and Surface Displacement. *Bulletin of the Seismological Society of America*, *84*(4), 974–1002.

Wendt, J., Oglesby, D. D., & Geist, E. L. (2009). Tsunamis and splay fault dynamics. *Geophysical Research Letters*, *36*, L15303. https://doi.org/10.1029/2009GL038295

Winston, J. G. (1983). Kodiak Shelf, Gulf of Alaska. In A. W. Bally (Ed.), Seismic expression of structural styles: A picture and work atlas: American Association of Petroleum Geologists Studies in Geology. (Vol. 15, pp. 140–146).

Witter, R. C., Briggs, R. W., Engelhart, S. F., Gelfenbaum, G., Kochler, R. D., & Barnhart, W. D. (2014). Little late Holocene strain accumulation and release on the Aleuri8an megathrust below the Shumagin Islands, Alaska. *Geophysical Research Letters*, *41*, 2359–2367. https://doi.org/10.1002/2014GL059393

Ye, S., Flueh, E. R., Klaeschen, D., & von Huene, R. (1997). Crustal structure along the EDGE transect beneath the Kodiak shelf off Alaska derived from OBH seismic refraction data. *Geophysical Journal International*, *130*, 283–302.

Zheng, G., Dmowska, R., & Rice, J. R. (1996). Modeling earthquake cycles in the Shumagin subduction segment, Alaska, with seismic and geodetic constraints. *Journal of Geophysical Research*, *101*(B4), 8383–8392.

Zimmermann, M., & Prescott, M. M. (2015). Smooth sheet bathymetry of the central Gulf of Alaska. NOAA Technical Memorandum NMFS-AFSC US Department of Commerce, National Marine Fisheries Service, Alaska Fisheries Science Center (Vol. 278). https://doi.org/10.7289/V5GT5D4F